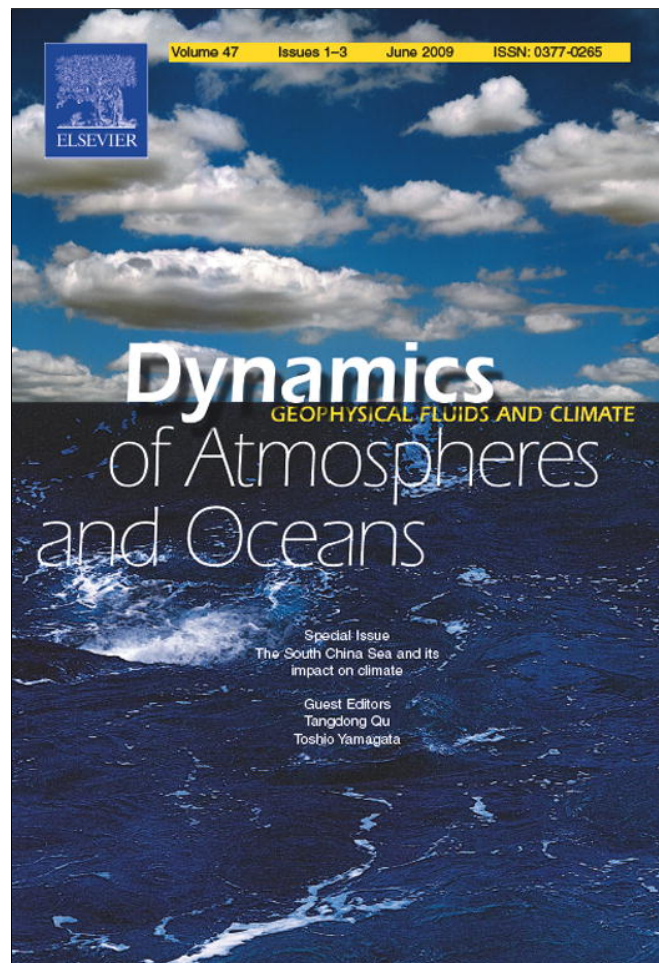


Provided for non-commercial research and education use.  
Not for reproduction, distribution or commercial use.



This article appeared in a journal published by Elsevier. The attached copy is furnished to the author for internal non-commercial research and education use, including for instruction at the authors institution and sharing with colleagues.

Other uses, including reproduction and distribution, or selling or licensing copies, or posting to personal, institutional or third party websites are prohibited.

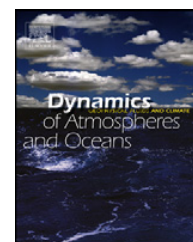
In most cases authors are permitted to post their version of the article (e.g. in Word or Tex form) to their personal website or institutional repository. Authors requiring further information regarding Elsevier's archiving and manuscript policies are encouraged to visit:

<http://www.elsevier.com/copyright>



Contents lists available at ScienceDirect

## Dynamics of Atmospheres and Oceans

journal homepage: [www.elsevier.com/locate/dynatmoce](http://www.elsevier.com/locate/dynatmoce)

# Seasonal surface ocean circulation and dynamics in the Philippine Archipelago region during 2004–2008

Weiying Han<sup>a,\*</sup>, Andrew M. Moore<sup>b</sup>, Julia Levin<sup>c</sup>, Bin Zhang<sup>c</sup>,  
Hernan G. Arango<sup>c</sup>, Enrique Curchitser<sup>c</sup>, Emanuele Di Lorenzo<sup>d</sup>,  
Arnold L. Gordon<sup>e</sup>, Jialin Lin<sup>f</sup>

<sup>a</sup> Department of Atmospheric and Oceanic Sciences, University of Colorado, UCB 311, Boulder, CO 80309, USA

<sup>b</sup> Ocean Sciences Department, University of California, Santa Cruz, CA, USA

<sup>c</sup> IMCS, Rutgers University, New Brunswick, NJ, USA

<sup>d</sup> EAS, Georgia Institute of Technology, Atlanta, GA, USA

<sup>e</sup> Lamont-Doherty Earth Observatory, Columbia University, Palisades, NY, USA

<sup>f</sup> Department of Geography, Ohio State University, Columbus, OH, USA

### ARTICLE INFO

#### Article history:

Available online 3 December 2008

#### Keywords:

Philippine Archipelago  
Straits  
Circulation and dynamics  
Transport

### ABSTRACT

The dynamics of the seasonal surface circulation in the Philippine Archipelago (117°E–128°E, 0°N–14°N) are investigated using a high-resolution configuration of the Regional Ocean Modeling System (ROMS) for the period of January 2004–March 2008. Three experiments were performed to estimate the relative importance of local, remote and tidal forcing. On the annual mean, the circulation in the Sulu Sea shows inflow from the South China Sea at the Mindoro and Balabac Straits, outflow into the Sulawesi Sea at the Sibutu Passage, and cyclonic circulation in the southern basin. A strong jet with a maximum speed exceeding 100 cm s<sup>-1</sup> forms in the northeast Sulu Sea where currents from the Mindoro and Tablas Straits converge. Within the Archipelago, strong westward currents in the Bohol Sea carry the surface water of the western Pacific (WP) from the Suri-gao Strait into the Sulu Sea via the Dipolog Strait. In the Sibuyan Sea, currents flow westward, which carry the surface water from the WP near the San Bernardino Strait into the Sulu Sea via the Tablas Strait.

These surface currents exhibit strong variations or reversals from winter to summer. The cyclonic (anticyclonic) circulation during winter (summer) in the Sulu Sea and seasonally reversing currents within the Archipelago region during the peak of the winter

\* Corresponding author at: Department of Atmospheric and Oceanic Sciences, University of Colorado, UCB 311, Stadium Room 255, Boulder, CO 80309, USA. Tel.: +1 303 735 3079; fax: +1 303 492 3524.

E-mail address: [Weiying.han@colorado.edu](mailto:Weiying.han@colorado.edu) (W. Han).

(summer) monsoon result mainly from local wind forcing, while remote forcing dominates the current variations at the Mindoro Strait, western Sulu Sea and Sibutu passage before the monsoons reach their peaks. The temporal variations (with the mean removed), also referred to as anomalies, of volume transports in the upper 40 m at eight major Straits are caused predominantly by remote forcing, although local forcing can be large during some-time of a year. For example, at the Mindoro Strait, the correlation between the time series of transport anomalies due to total forcing (local, remote and tides) and that due only to the remote forcing is 0.81 above 95% significance, comparing to the correlation of 0.64 between the total and local forcing. Similarly, at the Sibutu Passage, the correlation is 0.96 for total versus remote effects, comparing to 0.53 for total versus local forcing. The standard deviations of transports from the total, remote and local effects are 0.59 Sv, 0.50 Sv, and 0.36 Sv, respectively, at the Mindoro Strait; and 1.21 Sv, 1.13 Sv, and 0.59 Sv at the Sibutu Passage. Nonlinear rectification of tides reduces the mean westward transports at the Surigao, San Bernardino and Dipolog Straits, and it also has non-negligible influence on the seasonal circulation in the Sulu Sea.

© 2008 Elsevier B.V. All rights reserved.

## 1. Introduction

The multitude of straits and seas of the Philippine Archipelago comprises a region characterized by complex topography (see Fig. 1). This region is subject to strong seasonally reversing monsoon wind forcing: the northeast monsoon (NEM) during boreal winter and southwest monsoon (SWM) during boreal summer (Fig. 2). In addition, the circulations near the straits and seas of the Philippine Archipelago are strongly influenced by the circulations of the neighboring tropical Pacific Ocean and the South China Sea (SCS). The complexity of topography and strong winds present challenges for both observation and model simulations. As a consequence, the circulation and dynamics within the seas, in and around major straits are poorly understood.

Wyrtki (1961) reported the seasonal cycle of surface currents in the Southeast Asian waters based on available observations (Fig. 1). He suggested that throughout the year, surface water from the

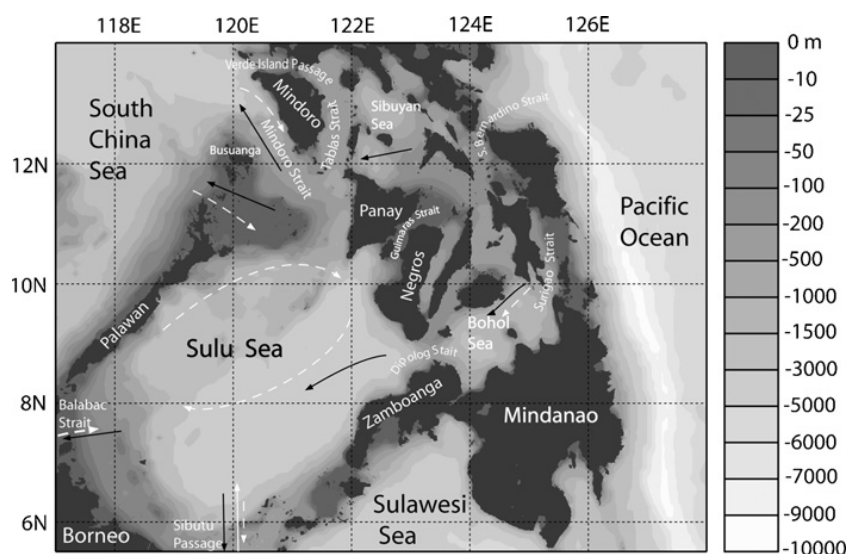


**Fig. 1.** Topographic conditions of the Philippine Archipelago region and schematics showing the surface currents during the NEM (black arrows) and the SWM (white dashed arrows) from Wyrtki (1961). The white solid arrow at the Sibutu Passage indicates the April–June reversal. This region is the same as the ROMS model domain (117°E–128°E, 0°N–14°N), except that the southern boundary is placed at 5°N to improve the visualization of straits, islands and their labels.

western Pacific enters the Philippine Archipelago via the Surigao Strait, flows westward through the Bohol [Mindanao] Sea and exits into the Sulu Sea at the Dipolog Strait. During the peak of the NEM, water from the western Pacific can also enter the Archipelago via the San Bernardino Strait and then flows westward into the Sulu Sea. Subsequently, waters in the Sulu Sea exit to the SCS via the Mindoro Strait in the north and the Balabac Strait in the west, and to the Sulawesi Sea through the Sibutu passage in the south (Fig. 1, black arrows). During April–June, currents at the Sibutu passage reverse to flow northward into the Sulu Sea (Fig. 1, white solid arrow). During August–October, currents change directions again, flowing southward from the SCS into the Sulu Sea and from the Sulu Sea into the Sulawesi Sea (his Plates 2–5; white dashed arrows of Fig. 1). During the peak of the SWM, circulation within the Sulu Sea is anticyclonic. Quadfasel et al. (1990) analyzed data from a hydrographic section collected during 28 August–17 September 1988 and suggested that the Subtropical Lower Water and Northern Pacific Intermediate Water from the SCS intrude into the Sulu Sea at the Mindoro Strait at ~200 m and 400–800 m, respectively.

There are a few modeling efforts that simulate the large-scale surface circulation in the Southeast Asian Seas. Metzger and Hurlburt (1996) studied the coupled dynamics of the circulation among the SCS, the Sulu Sea, and the Pacific Ocean used a global, 1.5-layer reduced gravity model with  $0.5^\circ \times 0.5^\circ$  resolution and forced by Hellerman and Rosenstein (1983) monthly wind climatology. The authors showed that the general circulation patterns agree well with the surface circulations from higher resolution ( $1/8^\circ$  and  $1/16^\circ$  resolution) Ocean General Circulation Model (OGCM) with realistic bottom topography (see also Metzger and Hurlburt, 2001). They suggested that the annual mean circulation in the Sulu Sea is cyclonic, and currents flow into the Sulu Sea from the SCS at the Mindoro Strait and exit to the Sulawesi Sea via the Sibutu Passage.

Wajsowicz (1999) investigated the mean and seasonal variations of transports through the straits of the Southeast Asian seas using simple models based on Sverdrup dynamics (Sverdrup, 1947) and an OGCM with horizontal resolution of  $0.4^\circ$  in longitude and  $0.4 \cos \theta$  in latitude ( $\theta$ ). The vertically integrated annual mean transport from the OGCM solution showed inflows from the SCS into the Sulu Sea via the Mindoro and Balabac Straits, and outflow from the Sulu Sea into the Sulawesi Sea near the Sibutu Passage. Qu et al. (2004) analyzed a  $0.25^\circ \times 0.25^\circ$  resolution OGCM results, and suggested an annual mean SCS-to-Sulu Sea Mindoro throughflow, which carries about 30% of the SCS throughflow from the Luzon Strait (e.g., Shaw, 1991; Farris and Wimbush, 1996; Qu et al., 2000; Sheremet, 2001; Centurioni and Niiler, 2004; Hsueh and Zhong, 2004; Xue et al., 2004; Caruso et al., 2006; Yuan et al., 2006, 2007), exits into the Sulawesi Sea in the south (also see Qu et al., 2005, 2006; Wang et al., 2006). The rest of the Luzon Strait transport flows southward near the western boundary and leaves the SCS through the Karimata Strait (Qu et al., 2004).

It has been suggested that the time mean transport at the Luzon strait, and subsequently at the Karimata, Mindoro and Balabac Straits and Sibutu Passage, are remotely forced by the large-scale winds in the Pacific Ocean, based on the Sverdrup theory (Sverdrup, 1947) and multiple island rule (Godfrey, 1989; Wajsowicz, 1993, 1999). The estimated transport values at these straits using the island rule, however, are unrealistically large and are not reliable compared to the observations, owing to the strong mixing induced by tides and winds and the complex bottom topography in the Archipelago region (Wang et al., 2006; Wajsowicz, 1999). As part of the SCS throughflow system, the Mindoro throughflow exports a portion of the warmer and fresher SCS water and thus plays a role in keeping the SCS heat and salt balance (Qu et al., 2005, 2006).

High-resolution modeling studies on the detailed circulation, dynamics and seasonal variations in the Philippine Archipelago region do not exist. The goal of this paper is to understand the seasonal surface circulation and dynamics within and around the Philippine Archipelago. The approach is to perform OGCM experiments using a high-resolution configuration of the Regional Ocean Modeling System (ROMS) that can resolve the major straits in the complex topographic region. An improved understanding of the near strait circulation and dynamics is necessary, because it is not only of scientific interest, but also relevant for the safe operation of marine vessels and environmental surveys by autonomous vehicles. Moreover, variations of the circulation near the Philippine Archipelago may have important implications for climate, because the Mindoro Strait current is part of the heat and freshwater conveyor in the western Pacific Ocean (e.g., Qu et al., 2006).

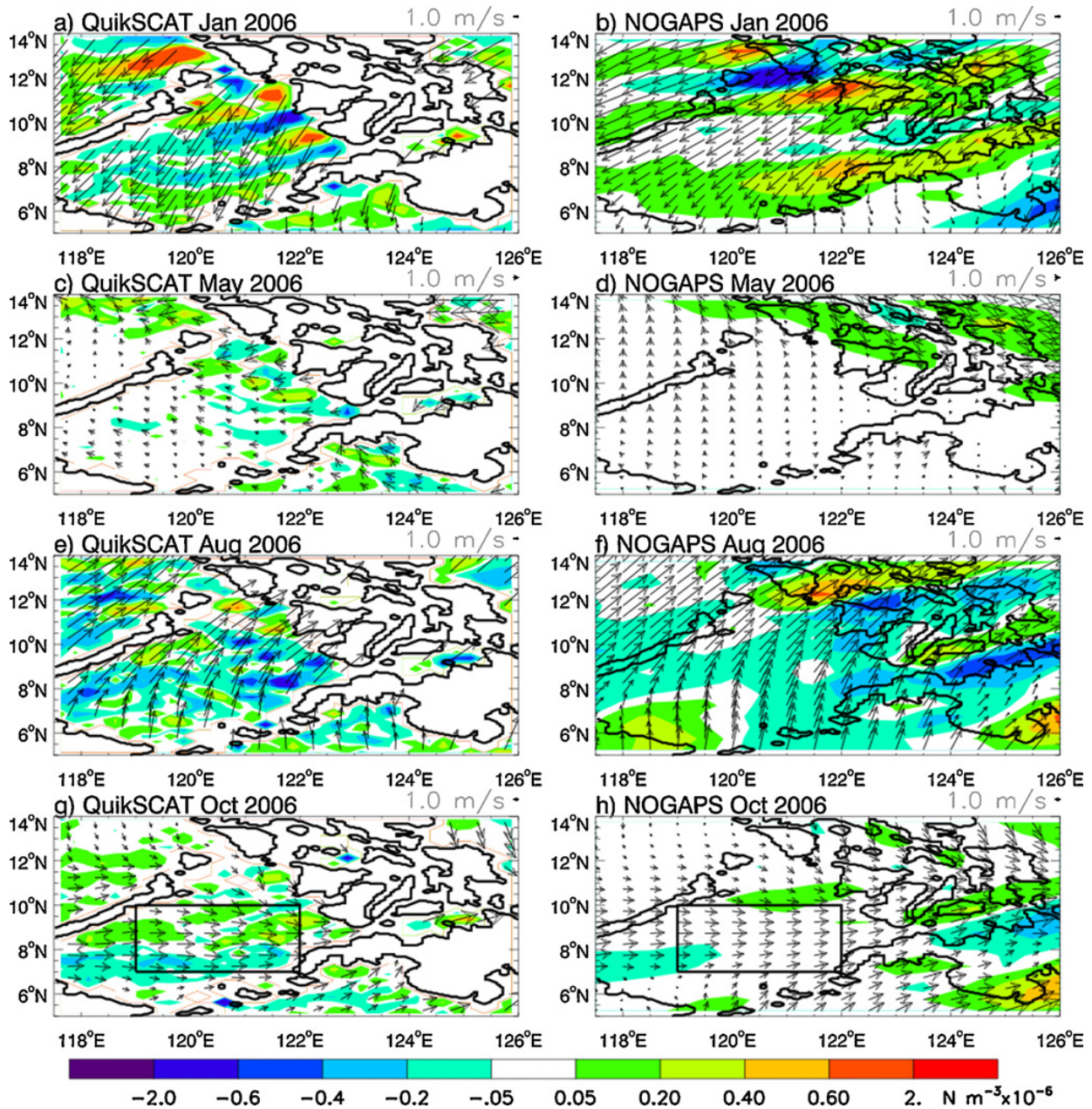


**Fig. 2.** Monthly mean wind at 10 m (arrows) and surface wind stress curl (color) for January, May, August and October 2006 from QuikSCAT data (left panel) and from the NOGAPS winds (right). The boxes in the Sulu Sea in g) and h) are used to form time series in Fig. 3.

## 2. Data and model

### 2.1. Satellite and in situ data

The 3-day mean,  $0.25^\circ \times 0.25^\circ$  resolution winds from the QuikSCAT Satellite are analyzed and compared with the Navy's Operational Global Atmospheric Prediction System (NOGAPS) winds which are used to force ROMS (see Section 2.2). In situ currents from the Philippine Archipelago Experiment (PhilEx) cruises during 9 January–1 February 2008 winter monsoon and June–July 2007 summer monsoon are analyzed and compared with the ROMS solution (Section 3.2). The summer data include two periods: 5 June–12 June (day 156–163) and 12 June–2 July of 2007 (day 163–183). The currents were from the Acoustic Doppler Current Profiler (ADCP) hull mounted system averaged for the 30, 40 and 50 m bins, and represent the average of 25–55 m.

**Table 1**

The three experiments performed: the Control Run (CR), Experiment 1 (EXP1) and Experiment 2 (EXP2). See Section 2.2.3 for detailed descriptions.

Experiments	Description	Period of time
CR	Complete solution	2 January 2004–1 March 2008
EXP1	Fix lateral boundary to 2004–2006 mean	2 January 2004–31 December 2006
EXP2	Tidal forcing removed	2 January 2004–31 December 2006

## 2.2. The ROMS

### 2.2.1. Model and configuration

The ROMS is a state-of-the-art model that can be configured for any region of the world ocean ranging from local to basin scale. ROMS solves the incompressible, hydrostatic, primitive equations with a free sea surface, horizontal curvilinear coordinates, and a generalized terrain-following  $s$ -vertical coordinate that can be configured to enhance resolution at the sea surface or seafloor. Values of  $s$  are between  $-1$  and  $0$ , which represent the vertical distances from the surface measured as the fraction of the local water column thickness, with  $0$  and  $-1$  corresponding to the free surface and oceanic bottom, respectively. The model numerics are described in detail in Shchepetkin and McWilliams (2005), and it has been used to simulate the circulation in a variety of different regions of the world ocean (e.g., Haidvogel et al., 2000; Malanotte-Rizzoli et al., 2000; She and Klinck, 2000; MacCready and Geyer, 2001; Penven et al., 2000, 2001; Marchesiello et al., 2003; Di Lorenzo et al., 2004; Wang and Chao, 2004). Moore et al. (2004) developed the ocean prediction and analysis system based on the tangent linear and adjoint of the ROMS. In this paper, the ROMS is configured to ( $117^{\circ}\text{E}$ – $128^{\circ}\text{E}$ ,  $0^{\circ}\text{N}$ – $14^{\circ}\text{N}$ ) region with 5 km horizontal resolution and 42 vertical levels, a region that includes the Philippine Archipelago (Fig. 1).

### 2.2.2. Initialization, forcing and numerics

The ROMS was initialized from the solution to the  $1/12^{\circ} \times 1/12^{\circ}$ , global HYbrid Coordinate Ocean Model (HYCOM) (Bleck, 2002) on 2 January 2004. Lateral boundary conditions for the three dimensional fields were obtained from the same global model. At the surface, ROMS was forced by the  $0.5^{\circ} \times 0.5^{\circ}$ , 3-hourly NOGAPS winds, shortwave and longwave radiation, air temperature, air pressure, specific humidity and precipitation fields. Barotropic tides were applied at the lateral boundaries of the ROMS to both free surface and velocities. The tidal data were obtained from the global Oregon State University (OSU) Tidal Inversion Software (OTIS) based on the TOPEX/Poseidon and Jason satellite altimeter data (Egbert et al., 1994; Egbert and Erofeeva, 2002), which includes eight components of the semi-diurnal and diurnal tides (M2, S2, N2, K2, K1, O1, P1 and Q1).

The model uses third order upstream bias horizontal advection scheme and parabolic spline vertical advection scheme for momentum and tracer equations (Shchepetkin and McWilliams, 2005). Harmonic mixing along geopotential lines is applied to the tracers, while harmonic mixing along  $s$ -levels is applied to momentum. Generic Length Scale turbulence closure (Warner et al., 2005) is used to facilitate vertical mixing; and quadratic drag is applied at the bottom. Boundary conditions are: Chapman—for the free surface, Flather—for the barotropic velocities, and clamped for the three dimensional fields (Stevens, 1990). Surface wind stress and net heat flux were computed using a bulk flux parameterization (Liu et al., 1979) and the COARE algorithm of Fairall et al. (1996a,b).

### 2.2.3. Experiments

Three experiments were performed as described in Table 1. In the Control Run (CR), the ROMS is forced by the 3-hourly NOGAPS forcing fields and tides for the period of January 2004–March 2008. The initial and lateral boundary conditions are provided by the global HYCOM daily solution without (with) data assimilation for 2004–2006 (1 January 2007–March 2008). To shed lights on the remote forcing from the adjacent seas and the Pacific Ocean, Experiment 1 (EXP1) is performed for 2004–2006. It is the same as the CR except that the lateral boundary conditions were held fixed at their 3-year mean values. This solution excludes the effects of synoptic-to-interannual variations of

remote forcing, however it still includes the remote influence on the 3-year mean circulation and tidal forcing. Current anomalies (with the 3-year mean removed) in the Archipelago region from the difference solution,  $CR-EXP1$ , measure the remote influence from the circulations of the adjacent seas (mainly the SCS) and the Pacific Ocean that are driven by atmospheric forcing fields outside the ROMS model domain. To assess the nonlinear rectification effects of tides, Experiment 2 (EXP2) is performed for the period of 2004–2006, in which tidal forcing is removed. Otherwise it is the same as the CR for the same time frame. The difference,  $CR-EXP2$ , estimates tidal rectification onto both time mean and variations of circulation. Current anomalies from solution  $EXP2-(CR-EXP1)$  assess the effects of atmospheric forcing local to the ROMS model domain. In this paper, we primarily discuss seasonal variations.

### 3. Model/data comparison

In this section, we will first compare the NOGAPS winds with the QuikSCAT winds, and then compare the ROMS solutions with the PhilEx observations.

#### 3.1. Prevailing winds

During winter and early spring, the NEM winds prevail (Fig. 2a), and when the winds blow through straits, intense atmospheric jets form along the downwind sides. Associated with these jets is a wind stress curl that is negative to the right and positive to the left of the wind axis. For example, negative/positive wind stress curl forms near the Tablas Strait and extends  $\sim 100$ – $200$  km into the Sulu Sea. Similar patterns of wind stress curl are observed downwind of the Guimaras and Dipolog Straits. West of the Mindoro Island, positive wind stress curl associated with the wind jet is strong. In summer, winds reverse to become the SWM, and the wind stress curl is generally negative within the Sulu Sea (Fig. 2e). The spring and fall are the monsoon transition periods (Fig. 2c and g). Within the Archipelago and near coasts, QuikSCAT winds are not available due to land contamination.

The NOGAPS winds generally reproduce the observed seasonally reversing monsoon winds (Fig. 2, right column). In many areas, the NOGAPS winds also capture the observed positive/negative regions of wind stress curl. For example, the positive/negative wind stress curl near the Tablas Strait and west of the Mindoro Island during winter (Fig. 2a–b), and the generally negative wind stress curl in the Sulu Sea during summer (Fig. 2e–f) are present in both the QuikSCAT and NOGAPS data. From the Bohol [Mindanao] Sea to the Surigao Strait, positive wind stress curl during the NEM is apparent in the NOGAPS winds, and are also seen in QuikSCAT observations. These agreements may be partly because the QuikSCAT data have been assimilated into the NOGAPS model since 10 November 2004 [Timothy Hogan, pers. commun, 2007]. Significant discrepancies, however, exist. Generally, the NOGAPS winds have a larger easterly component than the QuikSCAT winds during the NEM (compare Fig. 2a–b). The negative/positive wind stress curl associated with the wind jet west of the Guimaras Strait are completely absent in the NOGAPS winds, probably due to the coarse resolution of the NOGAPS model grid.

To further quantify the signals and errors of the NOGAPS winds, Fig. 3 shows monthly mean time series of QuikSCAT and NOGAPS wind speed and wind stress curl averaged over the Sulu Sea during 2004–2006. Similar to the QuikSCAT data, the NOGAPS wind speed exhibits a seasonal cycle, and the correlation coefficient between the two curves is 0.88 above 95% significance. The correlation for the wind stress curl is 0.90. The NOGAPS wind speed, however, is systematically weaker than the QuikSCAT data, and the positive wind stress curl during winter is stronger than that of the QuikSCAT. These errors will result in errors in the ROMS solution, and thus partly account for some of the model/data discrepancies.

#### 3.2. Comparison with the PhilEx observations

Fig. 4a shows the observed near-surface currents averaged over 25–55 m in the Philippine Archipelago during January 2008. A southward current is observed at the Mindoro Strait, which is in the same direction as the suggested annual mean current and vertically integrated transport by

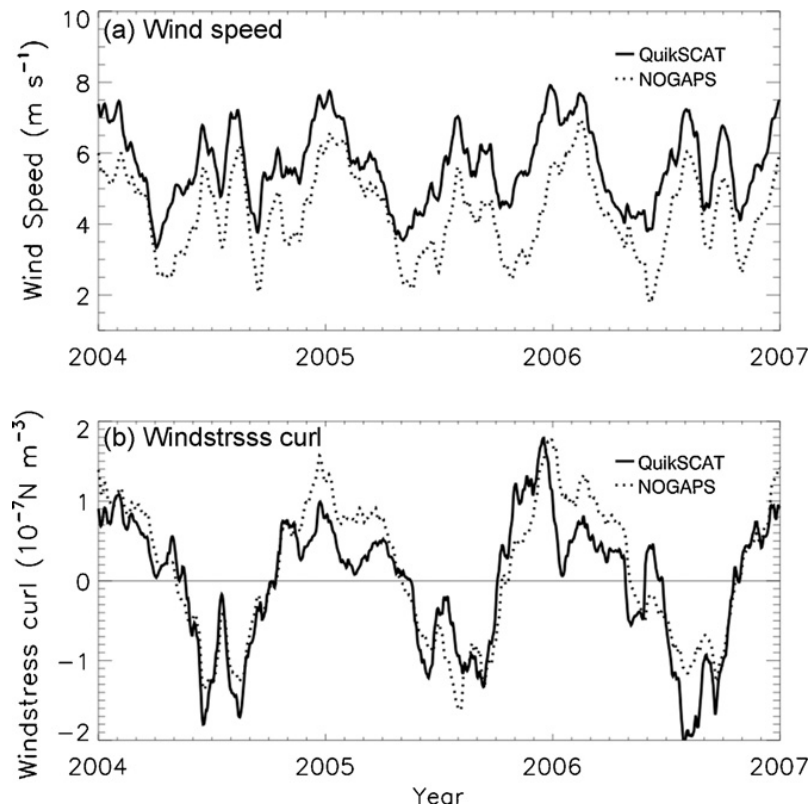


**Fig. 3.** (a) Time series of monthly mean QuikSCAT (solid curve) and NOGAPS (dotted curve) wind speed averaged over the Sulu Sea (boxed region in Fig. 2g–h) for 2004–2006; (b) same as (a) except for surface wind stress curl.

existing studies (see Section 1). A cyclonic eddy west of Mindoro near 13°N in the southeast SCS is present, and cyclonic eddies in this region had been studied by Wang et al. (2003, 2008) and Pullen et al. (2008). Both the southward Mindoro current and the cyclonic eddy are reasonably simulated in the ROMS CR (Fig. 4b). The southward Mindoro current, however, opposes the northward surface current suggested by Wyrтки for the NEM (c.f. Fig. 1). This discrepancy likely results from the lack of data in Wyrтки (1961) report. It is also possible that the ROMS solution and PhilEx observations are from shorter records than considered by Wyrтки. In both the model and observations, water from the western Pacific (WP) flows into the Archipelago at the Surigao and San Bernardino Straits. Subsequently, at the Surigao water from the WP flows westward in the Bohol Sea and exits into the Sulu Sea via the Dipolog Strait. There is a cyclonic eddy north of the Mindanao Island near 124°E. West of the San Bernardino, water in the Sibuyan Sea spreads westward, with part passing into the SCS via the Verde Island Passage. In the Sulu Sea west of the Panay Island, observed and simulated currents flow northward, and appear to be part of a cyclonic circulation. In the southeast Sulu Sea, the circulation is cyclonic in both the model and the observations.

During the summer PhilEx observational periods (Fig. 5), water from the WP enters the Bohol Sea through the Surigao Strait, flows westward, and discharges into the Sulu Sea at the Dipolog Strait in both the PhilEx data and the ROMS solution, as suggested by Wyrтки (1961) and similar to winter (Fig. 1). In the Bohol Sea north of the Zamboanga Peninsula, a cyclonic eddy is detected during the second period of the PhilEx observations. In the southeastern Sulu Sea, circulation is anticyclonic, in contrast to the cyclonic circulation during the winter monsoon (Fig. 4). Interestingly, the observed/simulated Mindoro Strait current reverses to flow northwestward comparing to the NEM, entering the SCS from the Sulu Sea. This flow is fed by the northward current along the west coast of Panay, and agrees with the April–June climatology of Wyrтки (1961). These summer currents are in contrast to the strong eddy flow pattern within Panay and Mindoro region observed in the winter monsoon.

The good qualitative agreements between the model and observations suggest that the ROMS is able to simulate the complex circulation within the Philippine Archipelago region in general,



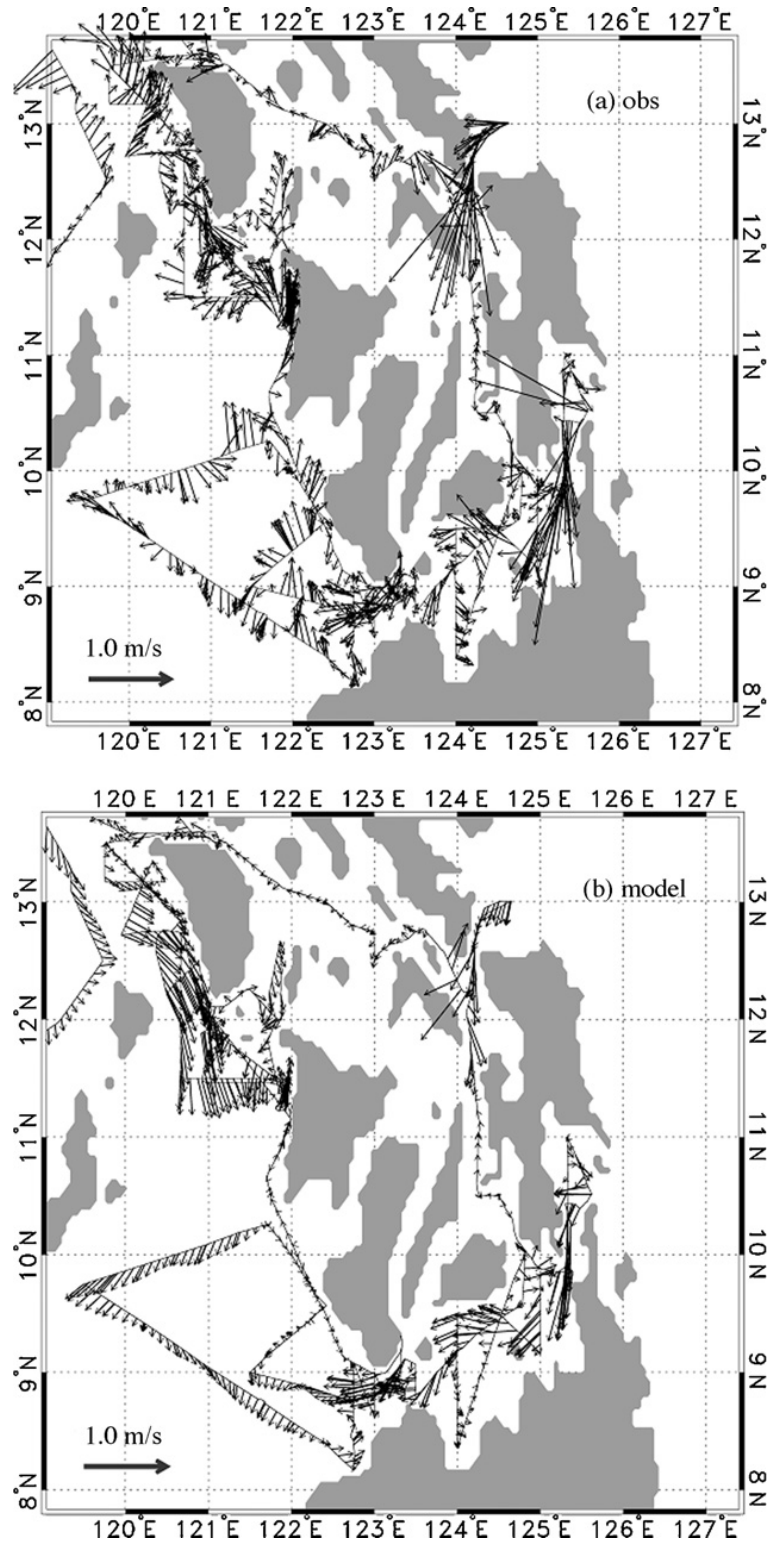


**Fig. 4.** (a) Observed currents averaged over 25–55 m depths from the PhilEx during 9 January–1 February 2008. (b) Same as (a) except for currents from the ROMS CR solution that are interpolated onto the 40 m depth and averaged over 9 January–1 February 2008.

and thus can serve the purpose of the present study. Note that compared to the  $1/12^\circ \times 1/12^\circ$  HYCOM solution that provided the initial and boundary conditions, the circulation of the ROMS CR is more energetic and is apparently better than HYCOM in a few areas of the model basin (not shown).

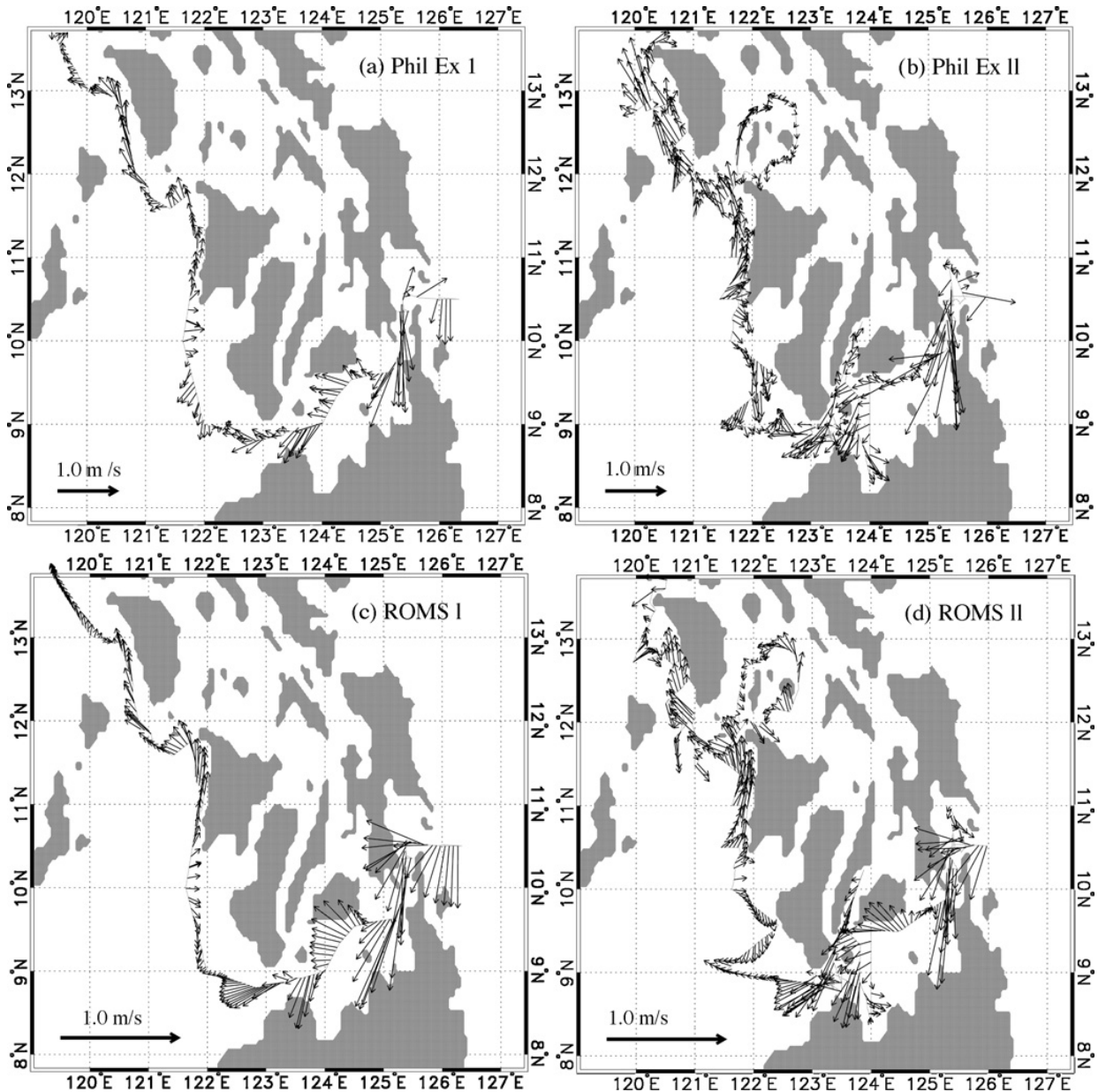


**Fig. 5.** (a) Observed currents averaged for 25–55 m from PhilEx period I (day 156–163 of 2007); (b) same as (a) except for period II (day 163–183 2007); (c) and (d) are the same as (a) and (b) except for the 40 m currents from the ROMS CR averaged over the corresponding PhilEx observational periods.

Significant model/data differences, however, exist. For example, during the NEM the simulated currents in the eastern Sulu Sea near the Guimaras Strait differ significantly from the observations (Fig. 4), where the NOGAPS wind stress curl has large errors (Fig. 2). Within the Sulu Sea, currents in the model are much weaker and lack some of the eddy features present in the data. Around the a few small Islands north of Panay, the ROMS solution shows a cyclonic circulation during the SWM (Fig. 5d), which is not observed by the PhilEx observations. These differences may result largely from errors in the NOGAPS forcing fields and the model errors. The model/data discrepancies may be also because, at least partly, the comparison between the time mean model currents over the observational periods versus the instant PhilEx data that contain aliases of synoptic variability and tidal currents. In the Tablas Sea, the observed northward currents during the NEM and SWM (Figs. 4a and 5b) are opposite to the model 40 m currents (Figs. 4b and 5d), but they agree well with the model surface currents (not shown). A possible explanation is that mixing of the model in this region might be too weak and thus surface momentum does not extend sufficiently deep.

## 4. Surface circulation and dynamics

### 4.1. Annual mean circulation

The annual mean surface currents and sea surface height (SSH) for 2004, 2005 and 2006 bear remarkable resemblance, albeit with quantitative variations from year to year (Fig. 6). Generally, the large-scale circulation in the Sulu Sea is dominated by the inflows from the SCS at the Mindoro and Balabac Straits, outflow into the Sulawesi Sea at the Sibutu Passage, and cyclonic circulation in the south Sulu basin. The Mindoro Strait inflow bends southwestward in the western Sulu basin, meets the eastward SCS water at the Balabac Strait, and a large portion exits into the Sulawesi Sea, with the rest returning to the Sulu Sea in the cyclonic gyre. This large-scale pattern is very similar to the annual mean circulation from the coarser resolution OGCM of Wajsowicz (1999) and Metzger and Hurlburt (1996), except that the latter has a closed Balabac Strait in their reduced gravity model. Within the Philippine Archipelago, one striking feature is the strong westward current in the Bohol Sea, which carries the surface water from the WP near the Surigao Strait into the Sulu Sea via the Dipolog Strait. In the Sibuyan Sea, the annual mean currents are directed westward and flow into the Sulu Sea via the Tablas Strait. Around the Islands north of Panay, the circulation is cyclonic. At the Verde Island Passage, surface water from the SCS intrudes into the Archipelago.

### 4.2. Seasonal variations

To provide a basin-scale picture of the temporal evolution of the surface circulation, Fig. 7 shows the monthly mean SSH and surface currents from the CR solution during the winter of 2005–2006 and summer of 2006. Given that the mean circulation for the 3 years are very similar (Fig. 6), we focus on discussing a specific year, and point out the major differences with the other 2 years.

The southward Mindoro Strait current, the subsequent southwestward flow in the Sulu Sea, the merging with the eastward Balabac Strait current, and the outflow into the Sulawesi Sea at the Sibutu Passage persist during the entire NEM and the peak of the SWM (Fig. 7a, b and d). An exception is the Balabac Strait current, which flows westward into the SCS in January. During June, however, the southward surface currents at the Mindoro Strait disappeared and at the Sibutu Passage reversed (Fig. 7c), the reversals being more apparent at 40 m depth (Fig. 8a). The reversed currents agree with the April–June climatology of Wyrтки (1961) and the PhilEx observations of June 2007, suggesting that this April–June reversal may be typical. The seasonal variations can also be seen in the near-surface (above 40 m depth) transports at the corresponding Straits (Fig. 9a–c, thick solid curves). During 2004 and 2005, no reversal occurs at the Mindoro Strait and the currents discussed above persist throughout the year (c.f. Fig. 8c).

The overall persistence of surface currents from the Mindoro Strait to the Sibutu Passage forms the strong annual mean pattern shown in Fig. 6. Within the Sulu Sea, the annual mean cyclonic gyre in the south-central basin results from the cyclonic circulations during the peak of both the NEM and SWM (Fig. 7a, b and d), although the route of the southwestward currents that carry the SCS water is pushed to the central Sulu basin during summer (Fig. 7d). In the northeast Sulu Sea, currents from the Mindoro and the Tablas Straits converge, forming a strong jet with a speed exceeding 100 cm/s during both the NEM and SWM (Fig. 7a and d).

Within the Philippine Archipelago, surface currents reverse directions with season (Fig. 7). During the NEM, currents in the Sibuyan Sea are directed northwestward, flowing into the Sulu Sea near the east coast of the Mindoro Island with a small portion entering the SCS via the Verde Island Passage in January. In summer, the SCS water intrudes into the Archipelago at the Verde Island Passage, and the circulation in the Sibuyan Sea is dominated by a cyclonic gyre. These currents dominate those of the NEM and are present in the annual mean (Fig. 6). Interestingly, the westward-flowing currents in the Bohol Sea during the NEM reverse during the peak of the SWM at the surface, whereas at 40 m depth they flow persistently westward throughout the year (Figs. 7 and 8), as shown in the observations (Figs. 4 and 5). This suggests that the surface Ekman layer is thin. The seasonal reversals of currents

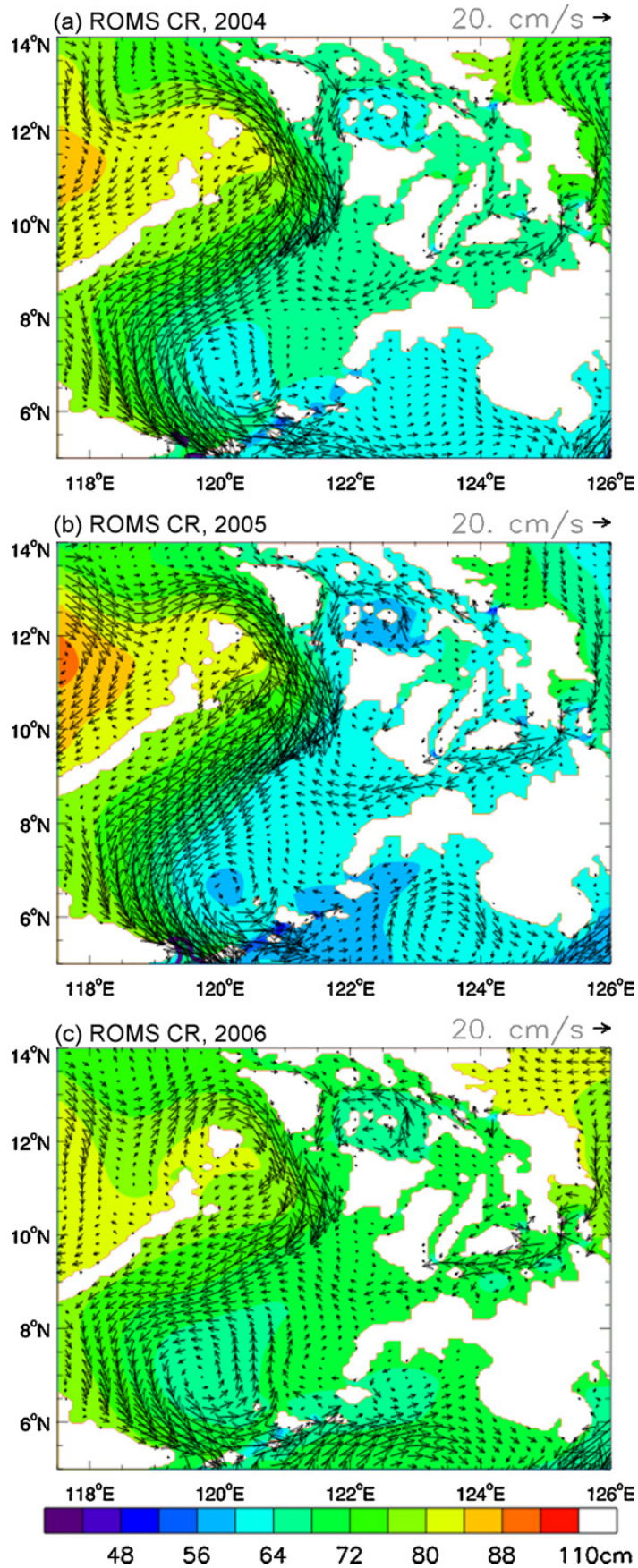


**Fig. 6.** Annual mean SSH (color contour) and surface currents (arrows) from the ROMS CR for (a) 2004, (b) 2005, and (c) 2006. The surface currents are the model's layer 1 currents with  $s = -0.0119$ . Arrows are plotted at every 5-grid point in zonal and 4-grid in meridional directions.

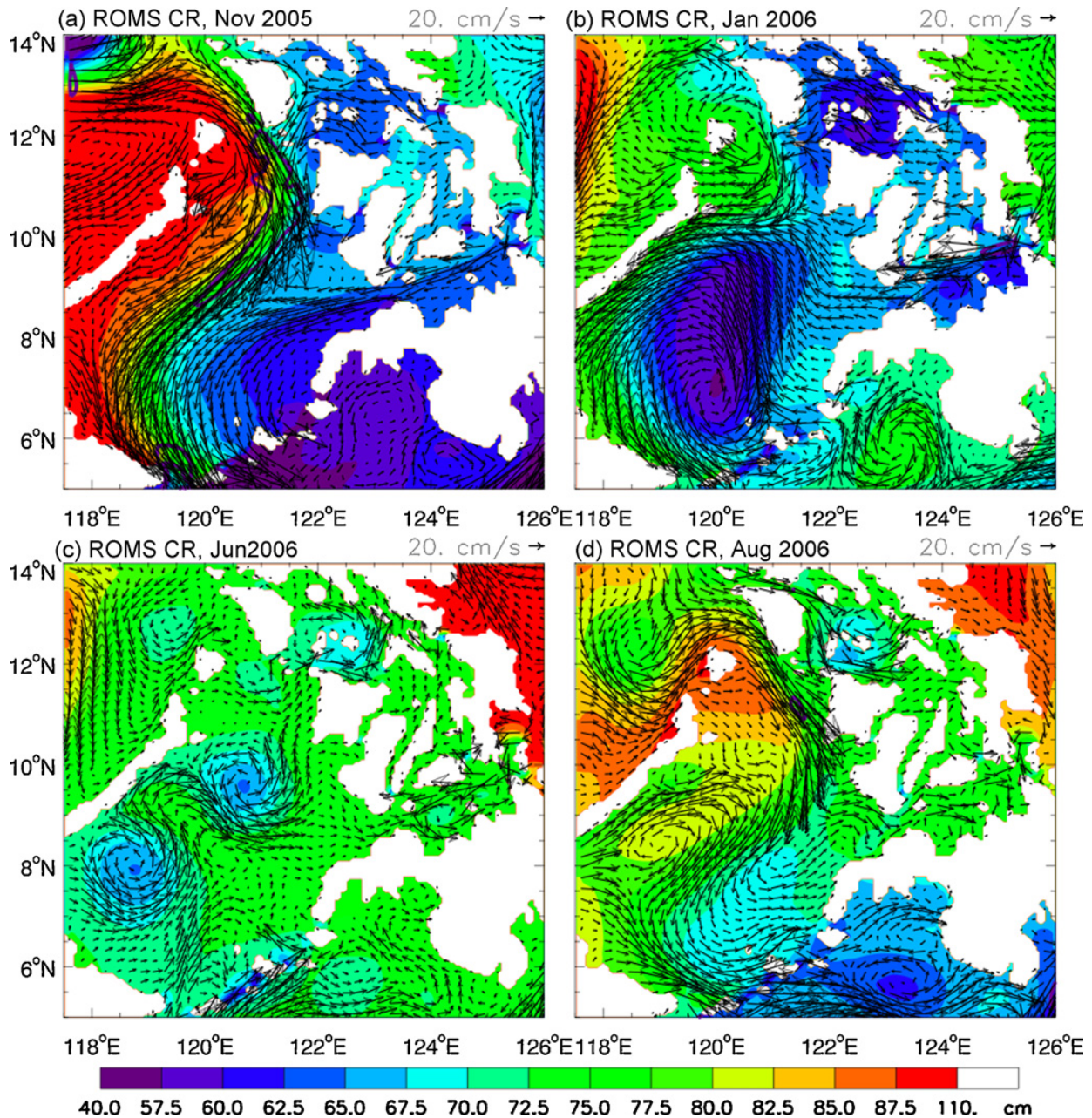


**Fig. 7.** (a) Monthly mean surface currents (arrows) and SSH (color contours) from the ROMS CR for November 2005; arrows are plotted at every 4-grid point in both zonal and meridional directions; current speeds greater than  $100 \text{ cm s}^{-1}$  are contoured by purple lines; (b), (c) and (d) are the same as (a) except for January, June and August 2006, respectively.

are also clearly seen in the transport time series at the Dipolog Strait, Tablas Strait and Verde Island Passage (Fig. 9d–f; thick solid lines).

As indicated by Figs. 6 and 7, surface inflows into the Sulu Sea from the Mindoro, Balabac, Tablas and Dipolog Straits are basically balanced by the outflow at the Sibutu Passage. This balance is quantified in Fig. 10, which shows that the total transport above 40 m depth at the four straits (thick solid line) is approximately balanced by the southward transport at the Sibutu Passage (thin solid line) on monthly timescales. The correlation coefficient between the two solid curves is 0.92 above 95% significance. The annual mean total transport values of the four straits for the upper 40 m depth are 2.3 Sv, 2.6 Sv and 1.5 Sv for 2004, 2005 and 2006, respectively, which are approximately balanced by the corresponding transports of 2.3 Sv, 2.5 Sv and 1.1 Sv at the Sibutu passage.

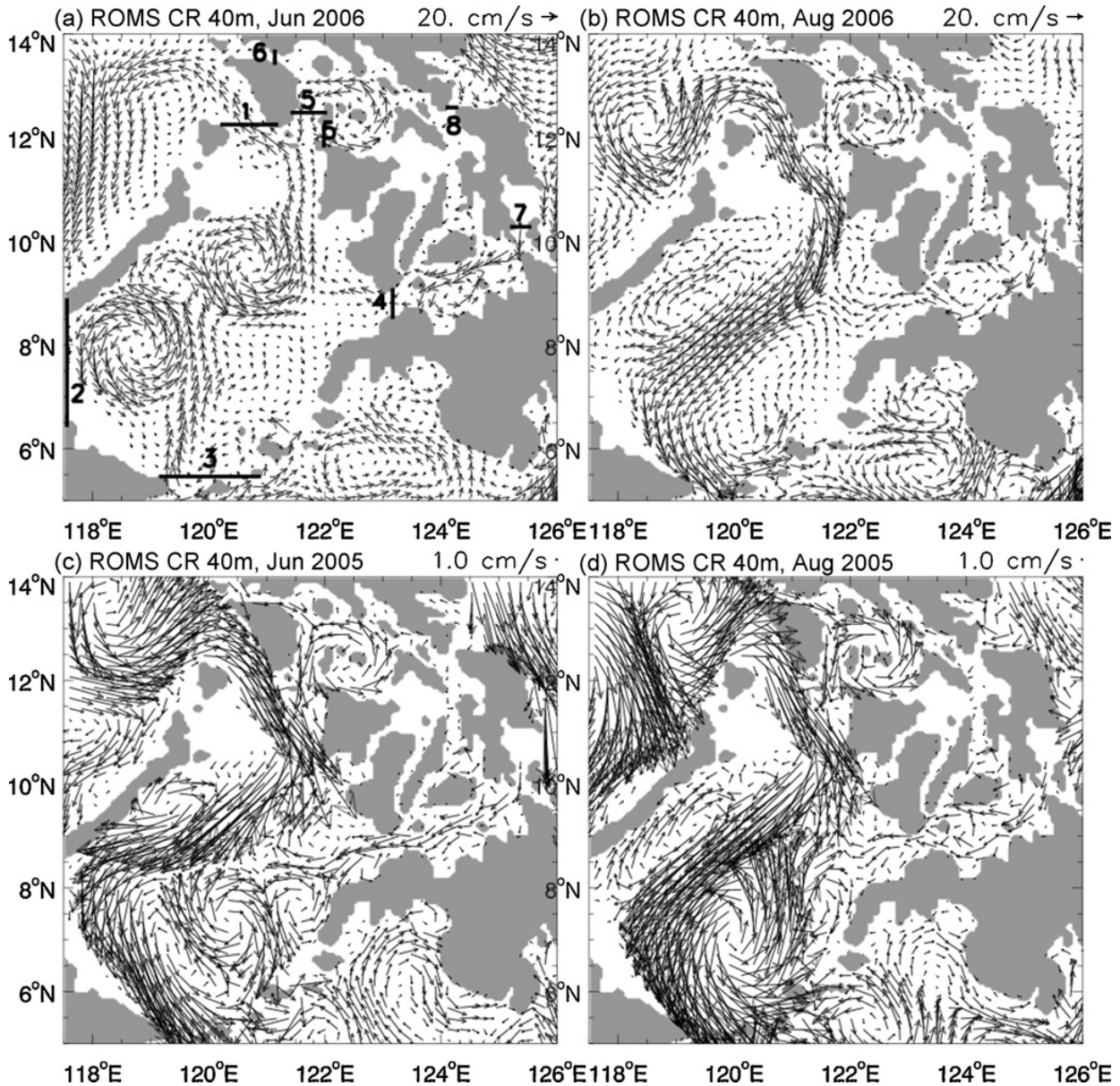


**Fig. 8.** Monthly mean currents at 40 m depth from the ROMS CR: (a) June 2006; (b) August 2006; (c) June 2005; (d) August 2005. Cross-sections at eight major straits are marked in (a), and the transport across each strait is shown in Fig. 9.

### 4.3. Dynamics

#### 4.3.1. Geostrophic current and Ekman drift

Note that the CR and EXP1 are designed to isolate the effects of remote versus local forcing on the “temporal variations” of the circulation rather than on the mean (Section 2.2.3). To shed light on the dynamics of the seasonal circulation with the mean included, we estimate the surface geostrophic current and Ekman drift (Fig. 11). The former is associated with the pressure gradient force and can be driven by both local and remote processes, while the latter is forced only by local wind stress. The geostrophic current is given by  $u_g = -(g/f)(\partial h/\partial y)$ ,  $v_g = (g/f)(\partial h/\partial x)$  where  $u_g, v_g$  are the zonal and meridional components,  $g = 9.8 \text{ m s}^{-2}$  is the acceleration of gravity,  $f$  is the Coriolis parameter, and  $h$  is SSH. The Ekman drift is estimated by  $u_e = \tau^y / f\rho H_e$ ,  $v_e = -(\tau^x / f\rho H_e)$ , where  $u_e$  and  $v_e$  are zonal and meridional components,  $\tau^x$  and  $\tau^y$  are zonal and meridional surface wind stress,  $\rho = 1000 \text{ kg m}^{-3}$  is water density and  $H_e$  is the Ekman layer thickness. For demonstration, we choose  $H_e = 20 \text{ m}$  in our calculation. Other values are also tested and the choice of  $H_e$  does not affect our qualitative discussion (see below). Note that the superposition of the geostrophic and Ekman components is much stronger than the total

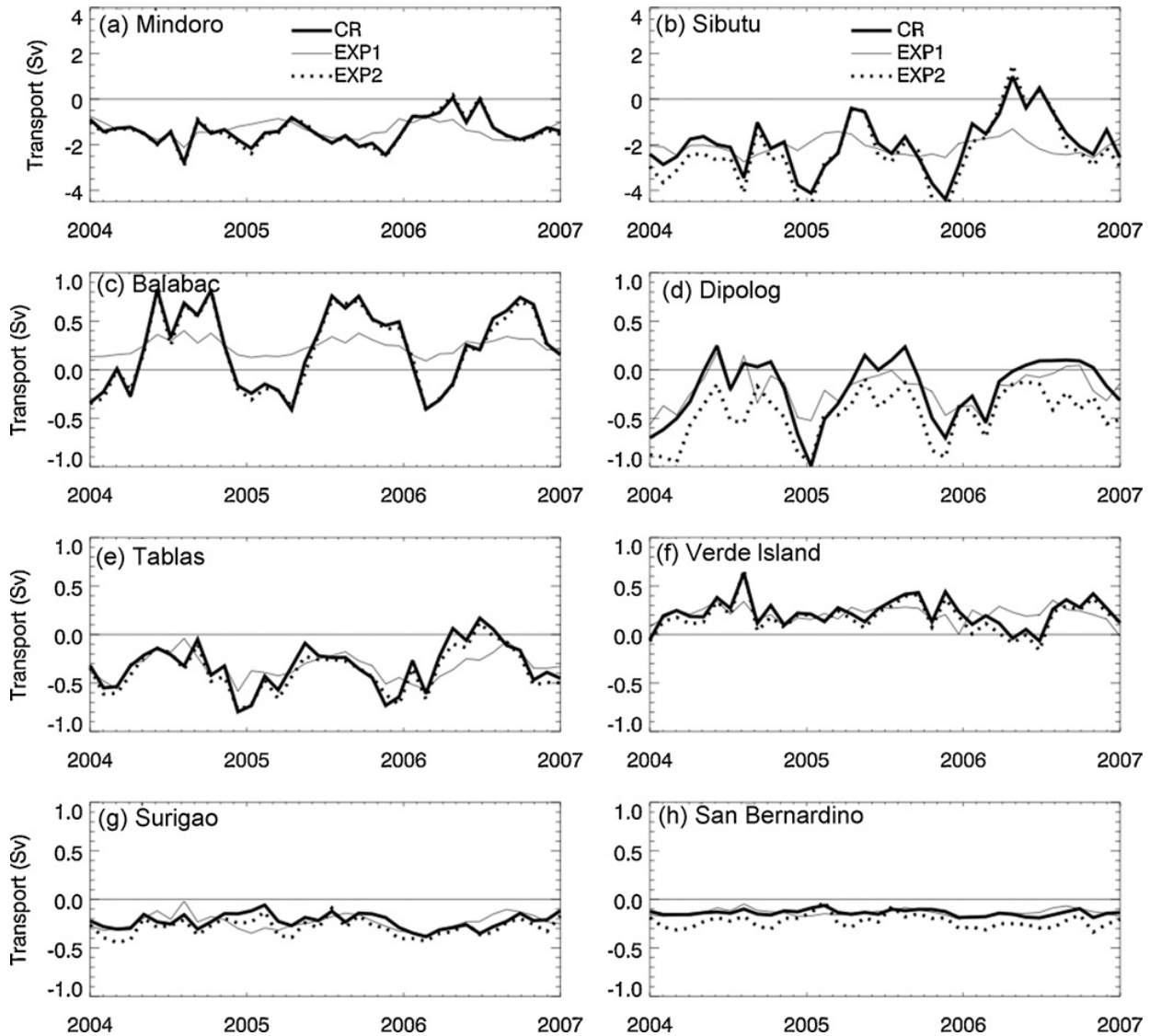


**Fig. 9.** Monthly mean across-strait transport above 40 m depth from the ROMS CR (thick solid), EXP1 (thin solid) and EXP2 (dotted) at each of the eight straits labeled in Fig. 8a. The thin solid and dotted lines will be discussed in Section 4.3.2.

model currents (compare Figs. 7 and 11). This suggests that nonlinearity and mixing are important in modifying the current amplitudes. In addition, near small straits such as the San Bernardino and Surigao Straits, there are a few unrealistically large values of geostrophic currents, suggesting that geostrophy may not hold there due to the strong influence of topography and tidal mixing.

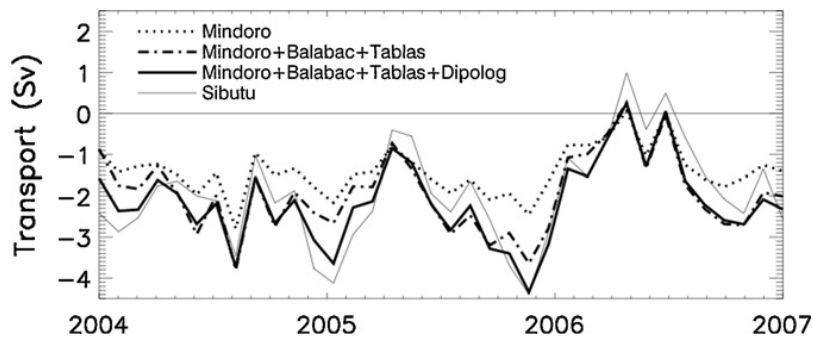


**Fig. 10.** Monthly mean across-strait transports above 40 m depth from the ROMS CR for the Mindoro Strait (dotted line), the sum of the Mindoro, Balabac and Tablas Straits (dash-dotted line), the sum of the Mindoro, Balabac, Tablas and Dipolog Straits (thick solid line), and the Sibutu Passage (thin solid line).

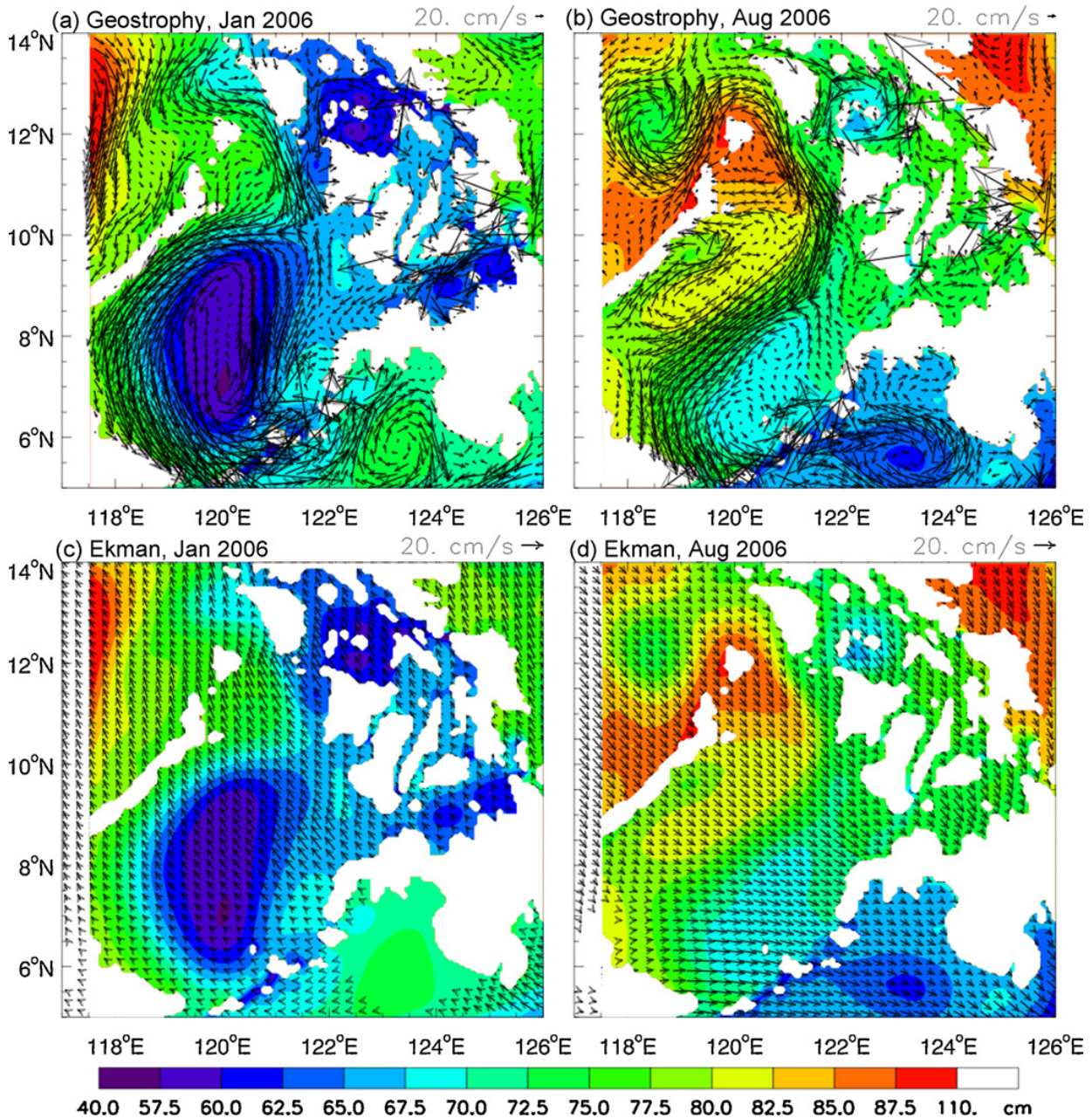


**Fig. 11.** (a) ROMS SSH and geostrophic currents during January 2006; (b) same as (a) except for August; (c) and (d) are the same as (a) and (b) except for Ekman drifts.

Evidently, the southward currents at the Mindoro Strait are dominated by the geostrophic component associated with the strong across-strait SSH gradients, while the Ekman drifts act to reduce the Mindoro Strait currents during the NEM but enhance them during the SWM. In the Sulu Sea, the surface circulation basically satisfies geostrophy, with the influence of the northwestward (southeastward) Ekman drifts during the NEM (SWM). The cyclonic eddy west of the Mindoro Island near 13.2°N in January (Fig. 7b) is in geostrophic balance (Fig. 11a), which is associated with the maximum positive wind stress curl there (Fig. 2b). It is also present in the winter of 2004–2005 of the ROMS solution (not shown). The regular occurrence of the eddy during the NEM further suggests that the positive wind stress curl is the major cause, a conclusion that is consistent with that of Pullen et al. (2008) and Wang et al. (2008).

In the Sibuyan Sea, geostrophic currents along the east coast of Mindoro Island flow into the Sulu Sea via the Tablas Strait during both the NEM and SWM (Fig. 11a and b). At the Verde Island Passage, the SCS water enters the Archipelago as geostrophic current during the SWM (Figs. 7d and 11b), and



water from the Archipelago flows into the SCS during January as Ekman drift (Figs. 4, 7b and 11c). In the east, both the Ekman and geostrophic components carry the water from the WP near the San Bernardino Strait into the Sibuyan Sea during winter, where most of it joins the southward geostrophic flow along the east coast of Mindoro and exits to the Sulu Sea. A geostrophic, cyclonic gyre dominates the circulation in the Archipelago north of Panay (Fig. 11a–b), and this forms its annual mean pattern (Fig. 6). It is associated with low SSH, which is mainly forced by the positive wind stress curl that lasts from May–September (cr. Fig. 1). As we shall see in Section 4.3.2, remote forcing also contributes to this gyre during summer.

In the Bohol Sea, the swift westward surface flow that carries the water from the WP into the Sulu Sea during the NEM is dominated by the geostrophic component (Fig. 11a). Of particular interest is that the strong currents flow near the northern boundary of the channel, where the SSH gradients are strong. This is mainly because the strong NEM winds cause northward Ekman transports (Fig. 11c), which pile up water along the northern boundary of the channel. As a result, a strong cross-channel gradient develops and a swift current or jet forms with a speed exceeding  $100 \text{ cm s}^{-1}$  during December–January (Fig. 7b). This along-channel flow favors the intrusion of the surface water from the WP. Geostrophic, cyclonic eddies frequently form north of the Mindanao Island (Figs. 4, 7 and 11), which coincide with the strong positive wind stress curl there (Fig. 2). The strong shear of the westward current, however, also acts to generate positive vorticity,  $\zeta = (\partial v / \partial x) - (\partial u / \partial y)$ , and favors the formation of cyclonic eddy via barotropic instability. In the above,  $\zeta$ ,  $u$ ,  $v$  are the relative vorticity, zonal and meridional current respectively. In contrast, during the SWM surface Ekman drifts are so strong that they push the water from the Sulu Sea into the Bohol Sea through the Dipolog Strait (Fig. 11d). This tends to increase the sea level in the south Bohol Sea, reverse the meridional SSH gradients and cause reversed geostrophic currents (Fig. 11b). The situation is very similar in 2005, except that the reversal of the Sulu-to-Bohol surface currents occurs in June instead of July.

#### 4.3.2. Seasonal variations: remote versus local forcing and tide

The seasonal variations of surface currents discussed above are more apparent when the mean is removed (Fig. 12). Interestingly, the seasonally reversing surface currents at the Mindoro Strait, Sibutu Passage and their associated flow in the Sulu Sea are strongly influenced by remote forcing, and are dominated by remote effects during November and June before the monsoons reach their peaks (Fig. 13). This result demonstrates that seasonal and interannual variations in the SCS (e.g., Chu et al., 1999) and the Pacific Ocean play an important role in controlling the Sulu Sea and Philippine Archipelago circulation. Remote effects also have a significant contribution to the currents near the Dipolog Strait, Tablas Strait, Verde Island passage and the cyclonic gyre north of Panay during the SWM. During January and August when the monsoon attain their peaks, local winds play a deterministic role in forcing the surface currents especially in the Philippine Archipelago region (Fig. 14). For example, the seasonally reversing currents in the Bohol Sea and Sibuyan Sea, the cyclonic eddy north of the Mindanao near  $124^\circ \text{E}$  during the NEM, the generally cyclonic circulation in the Sulu Sea in January and anticyclonic circulation in August result mainly from local wind forcing.

Diurnal and semi-diurnal tides can rectify into the mean and seasonal variations of currents, due to the nonlinear response of the ocean to the tidal forcing. Tidal rectification has a non-negligible effect on the Sulu Sea circulation (Fig. 15), perhaps through the effects of bottom topography and nonlinear advection that shift the locations of the jets and eddies. For example, the currents, meanders and their associated eddies in the Sulu Sea during June (Fig. 12c) are more energetic and located further east in EXP2, the solution without tides (not shown). The difference solution, CR–EXP2, produces the eddy features in the Sulu Sea as shown in Fig. 15. Within the Archipelago region, tides mainly act to reduce the mean westward surface currents in the Bohol Sea and the San Bernardino Strait, likely by strong mixing that weakens the SSH gradients. A detailed study on how and why tides affect the Archipelago circulation is beyond the scope of this study, but it is an essential aspect of our ongoing research.

To further quantify the effects of remote versus local forcing and tides, Fig. 9 shows the volume transports above 40 m across each of the eight major straits labeled in Fig. 8a from solution CR, EXP1 and EXP2. Consistent with the surface current analysis, tidal rectification acts to reduce the mean transports at the Dipolog, Surigao and San Bernardino Straits (compare the thick solid and dotted lines in Fig. 9d, g and h). Without tides (dotted curves), the westward transports are stronger. At other straits,

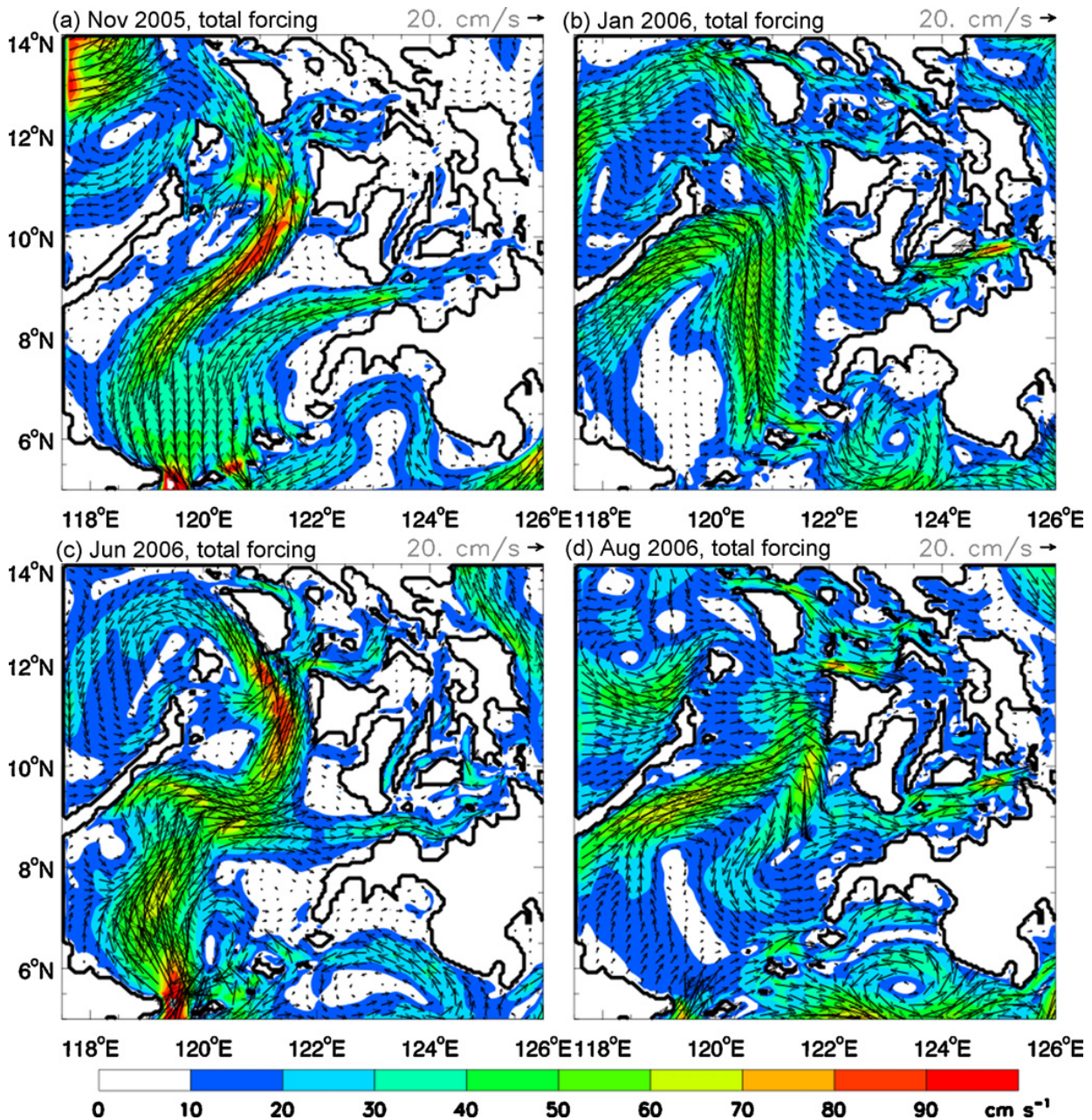


**Fig. 12.** Surface current anomalies from the ROMS CR, which include effects of all forcings. They are obtained by subtracting the mean of 2004–2006 from the monthly mean currents, and thus include both the seasonal cycle and year-to-year variations. Filled contours represent current amplitudes. (a) November 2005; (b) January 2006; (c) June 2006; (d) August 2006.

however, tidal influences are generally weak (Fig. 9a–c and e–f). Without the temporal variations of remote forcing (thin solid curves), variations of the transports are significantly altered especially at the Mindoro, Sibutu and Balabac Straits, and the April–June reversals of transport in 2006 at Sibutu, Mindoro, Tablas and Verde Island Passage shown in the CR (thick solid) did not occur in solution EXP1 (thin solid). This result is consistent with Fig. 13, which shows the large influence of remote forcing at these Straits and in the Sulu Sea.

Fig. 16 shows the transport anomalies (with the mean of 2004–2006 removed) due to remote and local forcing at six major straits where seasonal variations are relatively large. Note that the transport at each strait results from the effects of remote forcing, local forcing and tidal rectification. Evidently, variations of the near-surface transports at all these straits result predominantly from remote forcing (thick and thin solid lines), although the effects of local winds can be large during some times of a year (dotted lines). The correlation coefficients for total/remote (thick and thin solid lines) versus total/local

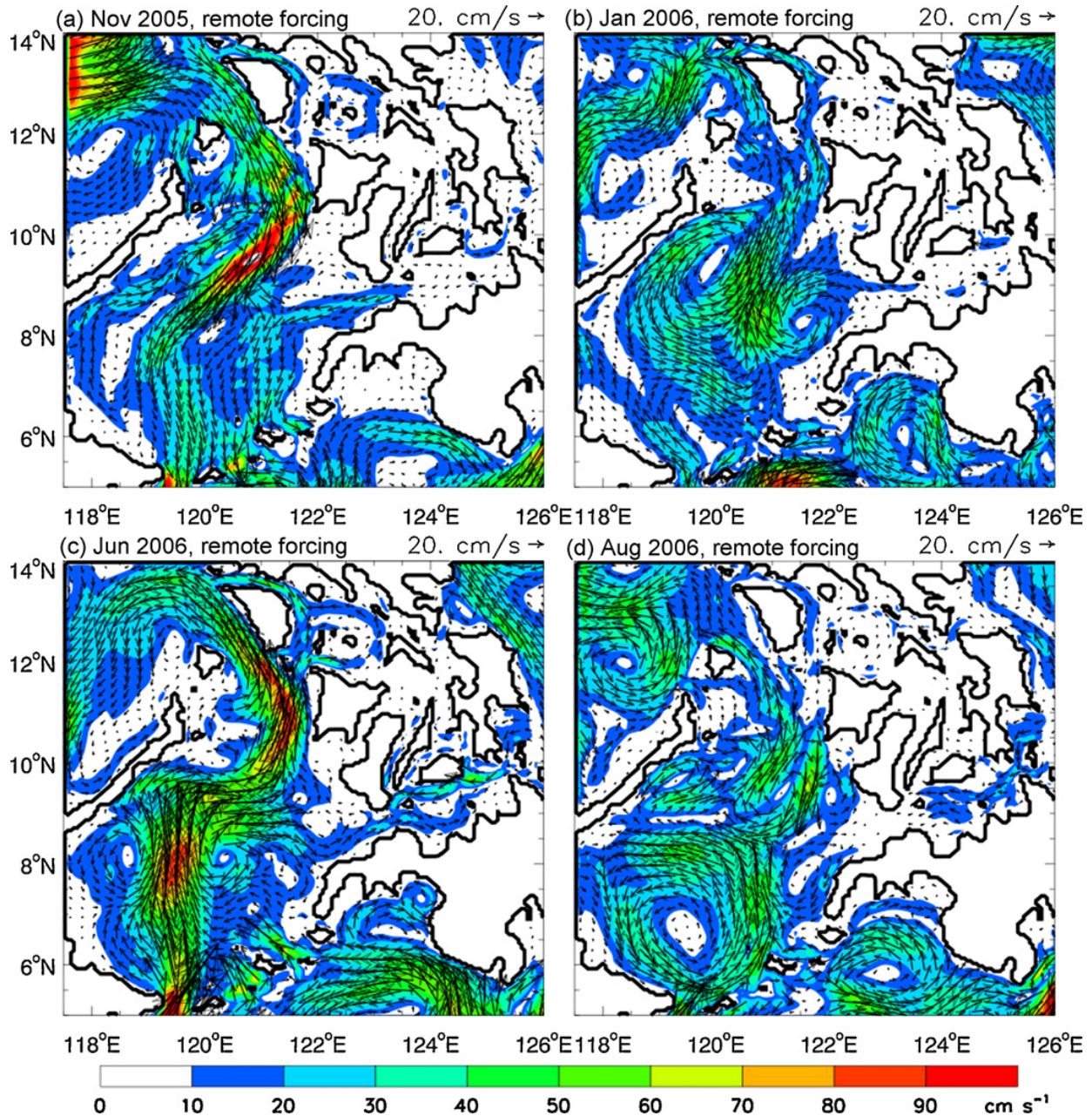


**Fig. 13.** Same as Fig. 12 except for surface current anomalies from the difference solution, *CR-EXP1*, which isolates the effects of remote forcing from the Pacific Ocean and the adjacent Seas.

(thick solid and dotted lines) are 0.81 versus 0.64 at the Mindoro Strait, 0.96 versus 0.53 at the Sibutu Passage, 0.996 versus 0.82 at Balabac Strait, 0.82 versus 0.49 at the Dipolog Strait, 0.81 versus 0.48 at the Tablas Strait, and 0.83 versus 0.52 at the Verde Island Passage. These correlation coefficients are above 95% significance. The standard deviation (S.D.) values of transports from the total, remote and local effects are 0.59 Sv, 0.50 Sv, and 0.36 Sv, respectively, at the Mindoro Strait; 1.21 Sv, 1.13 Sv, and 0.59 Sv at the Sibutu Passage; 0.40 Sv, 0.32 Sv, and 0.09 Sv at the Balabac Strait; 0.31 Sv, 0.18 Sv, and 0.16 Sv at the Dipolog Strait; 0.23 Sv, 0.18 Sv, and 0.15 Sv at the Tablas Strait; 0.15 Sv, 0.13 Sv, and 0.09 Sv at the Verde Island Passage.

These results suggest that even though local winds during the peak monsoon periods play a deterministic role in forcing surface currents (compare January and August panels of Figs. 12–14), remote influence dominates local forcing in determining the temporal variations of across-strait transports above 40 m (Fig. 16). This further suggests that the directly wind-driven Ekman layer is thin in the Archipelago region.

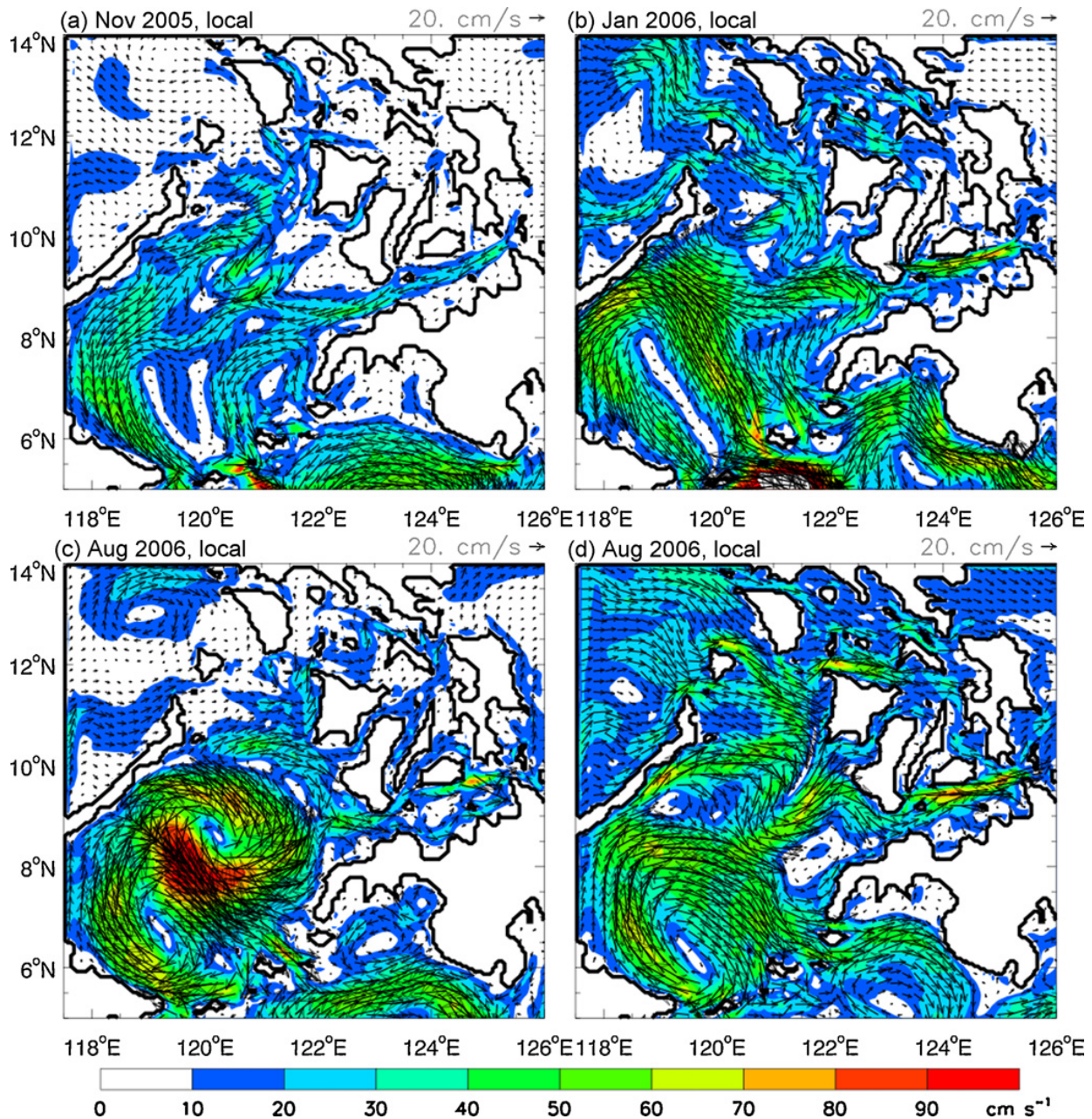


**Fig. 14.** Same as Fig. 12 except for surface current anomalies from the difference solution,  $EXP2-(CR-EXP1)$ , which isolates the effects of local forcing (see Section 2.2.3).

## 5. Summary and discussions

In this paper, we performed three experiments using a high-resolution configuration of the ROMS to understand the seasonal surface circulation and dynamics in and around the Philippine Archipelago region. The CR is performed for the period of January 2004–March 2008, and EXP1 and EXP2 are conducted for 2004–2006. These experiments are designed to assess the effects of remote versus local forcing and tidal rectification on the temporal variations of the Archipelago circulation (Table 1; Section 2.2). Surface currents from the CR agree reasonably with the PhilEx observations (Figs. 4 and 5).

The circulation in and around the Philippine Archipelago region is complex, with large temporal variations and energetic eddy activities. To the west, the Archipelago is connected to the SCS, Sulu Sea and Sulawesi Sea, and to the east it is connected to the Pacific Ocean (Fig. 1). Our results show that the southward surface currents at the Mindoro Strait and Sibutu Passage generally persist, although reversals often occur during April–June (Figs. 5–7, 9) as shown by Wyrтки (1961) climatology. These

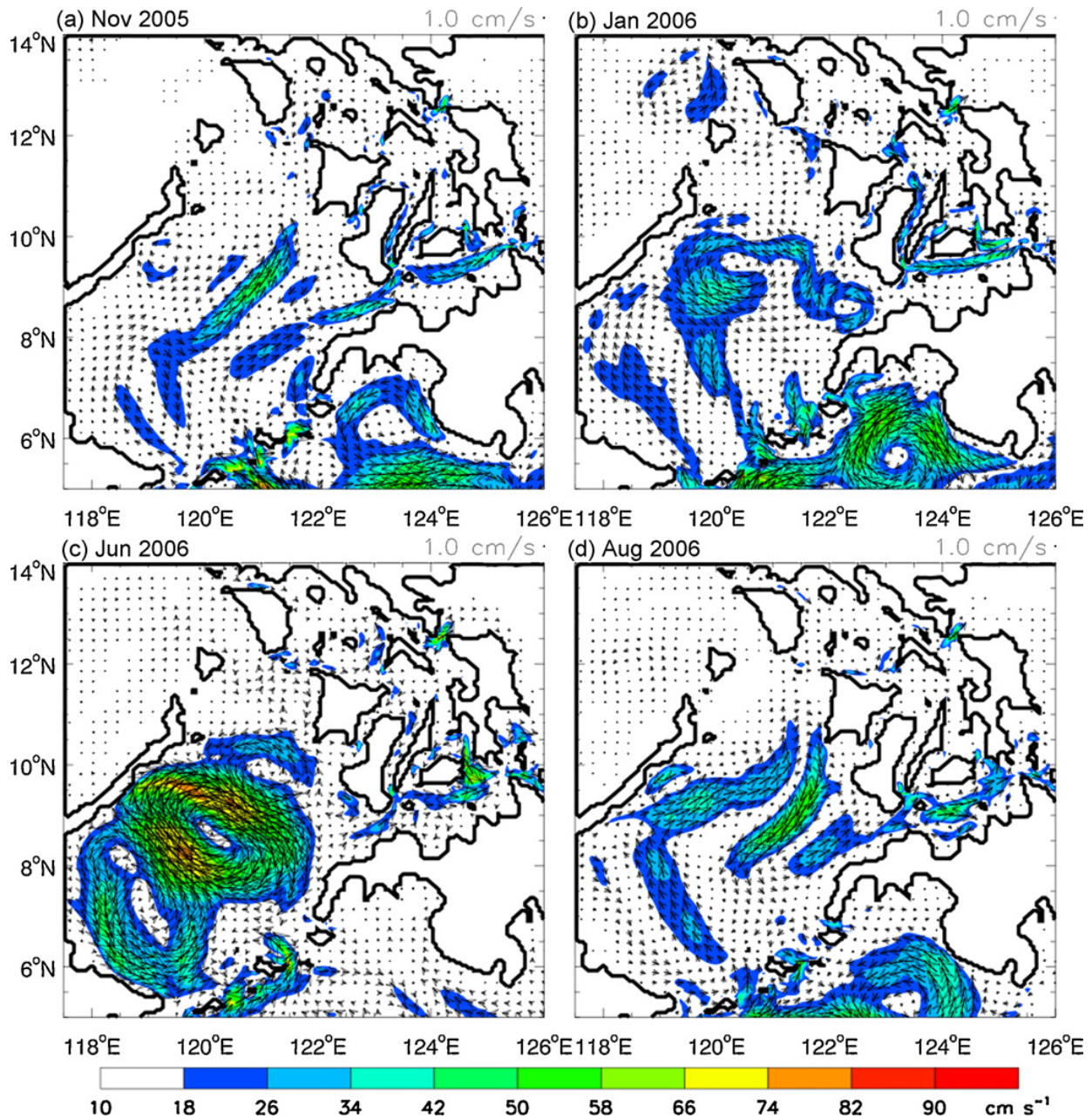


**Fig. 15.** Surface currents from the difference solution, *CR-EXP2*, which assess the tidal rectification onto the mean and variations of surface currents due to nonlinear response of the ocean to diurnal and semi-diurnal tide forcing. Filled contours represent current amplitudes.

persist currents form a strong annual mean pattern (Fig. 6), which transport the SCS water into the Sulawesi Sea, as suggested by previous studies. Our results also show that the eastward SCS water at the Balabac Strait, waters from the Archipelago at the Tablas and Dipolog Straits join the southwestward flow in the western Sulu Sea, with part entering the Sulawesi Sea and the rest returning to the Sulu Sea with the cyclonic gyre (Figs. 6 and 7; see Fig. 17 for a schematic illustration). These currents are generally dominated by geostrophic flow, with Ekman drift driven by the local winds contributing significantly during the monsoon peaks (Figs. 2, 3 and 11).

Within the Philippine Archipelago, the surface circulation reverses direction from the NEM to SWM (Fig. 7), and local winds play a deterministic role in causing the seasonal variations especially during the monsoon peak periods (Figs. 12–15). The observed cyclonic eddy north of Mindanao near 124°E during January is mainly forced by the positive wind stress curl (Figs. 2, 4 and 14), while the strong shear of the westward currents against the northern boundary of the Bohol Sea also favors the cyclonic eddy forma-

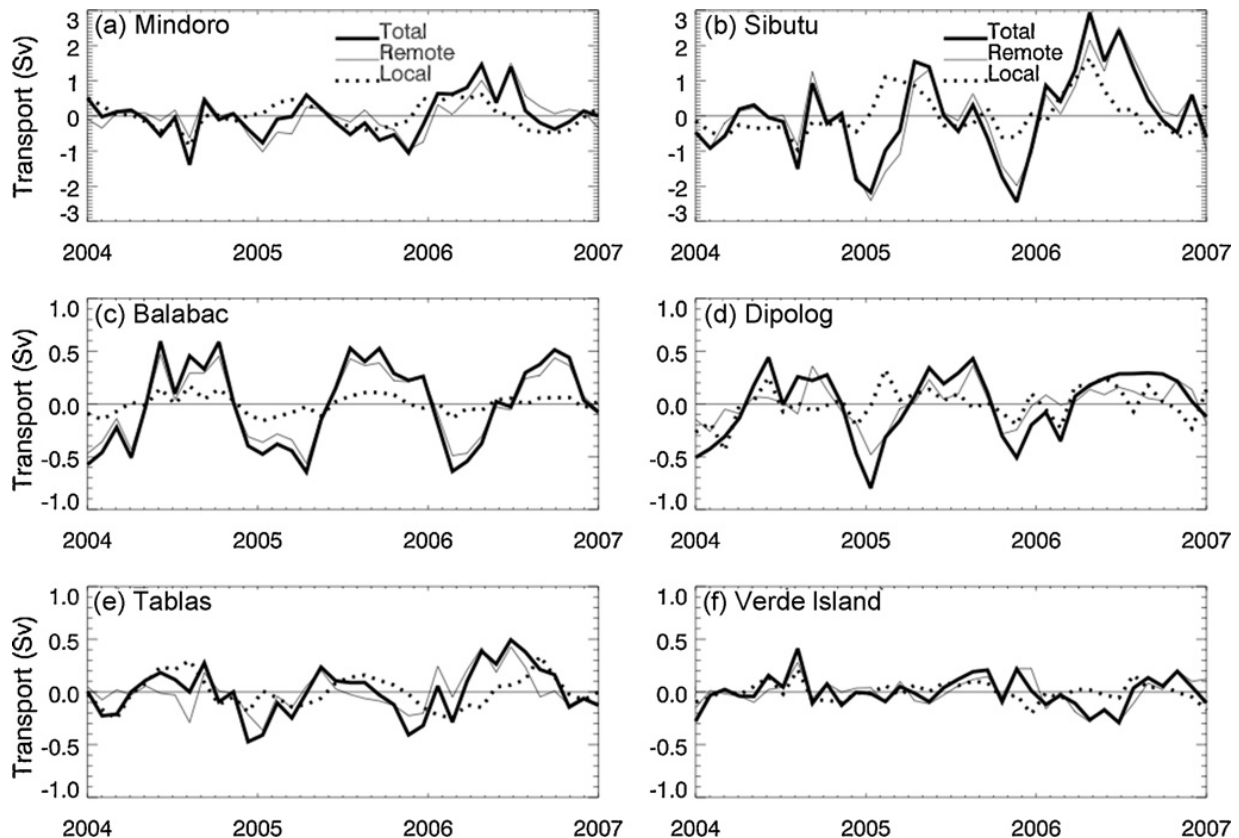


**Fig. 16.** Temporal variations of across-strait transport obtained by removing the corresponding 2004–2006 mean at each strait from the CR (thick solid lines), which represent “total” forcing,  $EXP2-(CR-EXP1)$ , which mainly estimates local forcing (dotted lines), and difference solution ( $CR-EXP1$ ), which represents remote forcing (thin solid lines).

tion. Although currents at the surface reverse to flow eastward in the Bohol Sea during the SWM (Fig. 7), currents at 40 m depth flow persistently westward throughout the year (Figs. 4, 5 and 8), suggesting that the Ekman layer is thin in our model. In the Sulu Sea, the cyclonic gyre during the peak of the NEM and anticyclonic circulation during the peak of the SWM result mainly from local wind forcing, with remote forcing having significant modification to the circulation (January and August of Figs. 12–14). Before the peak of the monsoons, remote forcing is the major cause for the surface currents in the Mindoro Strait, western Sulu Sea and the Sibutu Passage (November and June panels of Figs. 12–14).

Interestingly, although local winds play a crucial role in the Archipelago at the surface especially during the peak periods of monsoons, remote forcing dominates the seasonal variations of transports above 40 m at all the major straits and passages: Mindoro, Balabac, Dipolog, and Tablas Straits, as well as Sibutu and Verde Island Passages (Figs. 9 and 16). The correlation coefficients between the total transport anomalies (with the mean of 2004–2006 removed) and that due to the remote forcing only are 0.81, 0.996, 0.82, 0.81, 0.96 and 0.83 at each of the six straits or passages, which are in contrast to the correlations of 0.64, 0.53, 0.82, 0.49, 0.48 and 0.52 between the total and locally forced transport anomalies. In the upper 40 m, inflow transports into the Sulu Sea from the Mindoro, Balabac, Tablas and Dipolog Straits are approximately balanced by the outflow at the Sibutu Passage on monthly and annual timescales (Fig. 10; Section 4.2). These results demonstrate that remote forcing plays an important role in controlling the temporal variations of the transports across major straits within the Archipelago and the Sulu Sea. This suggests that a successful prediction of circulation and transport in and around the straits will not only require an accurate simulation of locally forced currents, but also remote effects from the SCS and the Pacific Ocean. Tidal rectification reduces the mean westward transports at the San Bernardino, Surigao and Dipolog Straits (Figs. 9 and 15), possibly because tidal mixing acts to weaken the pressure gradients at the Straits. Tides also affect the seasonal variations of the Sulu Sea circulation (Fig. 15), likely by shifting the locations of the jets and eddies and by tidal mixing.

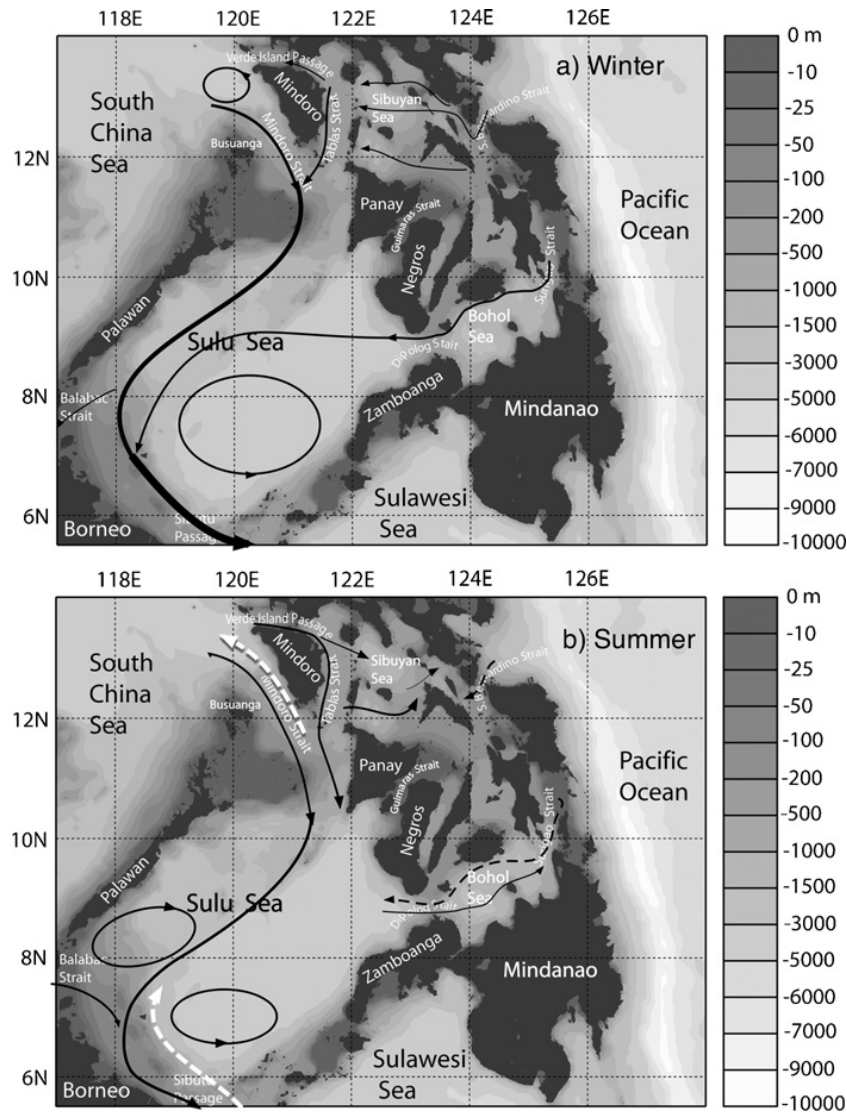


**Fig. 17.** Schematic diagram showing the surface circulation from the ROMS model during (a) winter, and (b) summer. The dark dashed lines at the San Bernardino Strait, Surigao Strait and in the Bohol Sea in (b) show the currents at 40 m depth during summer, which are opposite to the surface flow. The white dashed lines at the Sibutu Passage and Mindoro Strait in (b) indicate the April–June current reversals at 40 m, which occurred in 2006 and 2007 during our period of interest.

Here we report the detailed seasonal surface circulation and dynamics of the Philippine Archipelago region for the first time. Even though the successful simulation of circulation is encouraging, errors exist in the ROMS solution comparing with the observations. These errors may result partly from the coarse resolution and inaccuracy of the NOGAPS forcing fields, incorrect heat flux and freshwater parameterizations, and lack of river outflow in the model. Additionally, improving vertical mixing, lateral boundary conditions and bathymetry will also help to improve our future model simulations.

### Acknowledgements

The QuikSCAT winds are produced by Remote Sensing Systems and sponsored by the NASA Ocean Vector Winds Science Team (OVWST). Tide data are obtained at <http://www.coas.oregonstate.edu/research/po/research/tide/index.html>. We thank Dr. J. Metzger and Harley Hurlburt for providing the global HYCOM solutions, which are used as initial and lateral boundary conditions to the ROMS. Appreciation also goes to Dr. Phil Mele for processing the PhilEx ADCP data. Weiqing Han is supported by ONR N00014-07-1-0413 and NASA Ocean Vector Wind Science Team 1283568. Julia Levin, Bin Zhang, Hernan Arango and Enrique Curchitser by ONR N00014-07-1-0417, Arnold L. Gor-

don by ONR N00014-06-1-0689, and Jialin Lin by the NASA Modeling, Analysis and Prediction (MAP) Program.

## References

- Bleck, R., 2002. An oceanic general circulation model framed in hybrid isopycnic-cartesian coordinates. *Ocean Modeling* 4, 55–88.
- Caruso, M., Gawarkiewicz, G.G., Beardsley, R., 2006. Interannual variability of the Kuroshio Current intrusion in the South China Sea. *J. Oceanogr.* 62, 559–575.
- Centurioni, L.R., Niiler, P.P., 2004. Observations of inflow of Philippine Sea surface water into the South China Sea through the Luzon Strait. *J. Phys. Oceanogr.* 34, 113–121.
- Chu, P.C., Edmons, N.L., Fan, C., 1999. Dynamical mechanisms for the South China Sea seasonal circulation and thermohaline variabilities. *J. Phys. Oceanogr.* 29, 2971–2989.
- Di Lorenzo, E., Miller, A.J., Neilson, D.J., Cornuelle, B.D., Moisan, J.R., 2004. Modeling observed California current mesoscale eddies and the ecosystem response. *Int. J. Remote Sensing* 25 (7), 1307–1312.
- Egbert, G.D., Bennett, A., Foreman, M., 1994. TOPEX/Poseidon tides estimated using a global inverse model. *J. Geophys. Res.* 99, 24,821–24,852.
- Egbert, G.D., Erofeeva, S.Y., 2002. Efficient inverse modeling of barotropic ocean tides. *J. Atmos. Oceanic Technol.* 19 (2), 183–204.
- Farris, A., Wimbush, M., 1996. Wind-induced Kuroshio intrusion into the South China Sea. *J. Oceanogr.* 52, 771–784.
- Fairall, C.W., Bradley, E.F., Rogers, D.P., Edson, J.B., Young, G.S., 1996a. Bulk parameterization of air-sea fluxes for tropical ocean-global atmosphere Coupled-Ocean Atmosphere Response Experiment. *J. Geophys. Res.* 101, 3747–3764.
- Fairall, C.W., Bradley, E.F., Godfrey, J.S., Wick, G.A., Edson, J.B., Young, G.S., 1996b. Cool-skin and warm-layer effects on sea surface temperature. *J. Geophys. Res.* 101, 1295–1308.
- Godfrey, J.S., 1989. A Sverdrup model of the depth-integrated flow for the world ocean allowing for island circulations. *Geophys. Astrophys. Fluid Dyn.* 45, 89–112.
- Haidvogel, D.B., Arango, H.G., Hedstrom, K., Beckmann, A., Malanotte-Rizzoli, P., Shchepetkin, A.F., 2000. Model evaluation experiments in the North Atlantic basin: simulations in nonlinear terrain-following coordinates. *Dyn. Atmos. Oceans* 32, 239–281.
- Hellerman, S., Rosenstein, M.J., 1983. Normal monthly wind stress over the world ocean with error estimates. *J. Phys. Oceanogr.* 13, 1093–1104.
- Hsueh, Y., Zhong, L., 2004. A pressure-driven South China Sea Warm Current. *J. Geophys. Res.* 109, C09014, doi:10.1029/2004JC002374.
- Liu, W.T., Katsaros, K.B., Businger, J.A., 1979. Bulk parameterization of the air-sea exchange of heat and water vapor including the molecular constraints at the interface. *J. Atmos. Sci.* 36, 1722–1735.
- MacCready, P., Geyer, G.R., 2001. Estuarine salt flux through an isohaline surface. *J. Geophys. Res.* 106, 11629–11637.
- Malanotte-Rizzoli, P., Hedstrom, K., Arango, H.G., Haidvogel, D.B., 2000. Water mass pathways between the subtropical and tropical ocean in a climatological simulation of the North Atlantic ocean circulation. *Dyn. Atmos. Oceans* 32, 331–371.
- Marchesiello, P., McWilliams, J.C., Shchepetkin, A.F., 2003. Equilibrium structure and dynamics of the California current system. *J. Phys. Oceanogr.* 33, 753–783.
- Metzger, E.J., Hurlburt, H.E., 1996. Coupled dynamics of the South China Sea, the Sulu Sea, and the Pacific Ocean. *J. Geophys. Res.* 101, 12331–12352.
- Metzger, E.J., Hurlburt, H.E., 2001. The nondeterministic nature of Kuroshio penetration and eddy shedding in the South China Sea. *J. Phys. Oceanogr.* 31, 1712–1732.
- Moore, A.M., Arango, H.G., Di Lorenzo, E., Cornuelle, B.D., Miller, A.J., Neilson, D.J., 2004. A comprehensive ocean prediction and analysis system based on the tangent linear and adjoint of a regional ocean model. *Ocean Modelling* 7, 227–258.
- Penven, P., Roy, C., Colin de Verdiere, A., Largier, J., 2000. Simulation and quantification of a coastal jet retention process using a barotropic model. *Oceanol. Acta* 23, 615–634.
- Penven, P., Roy, C., Lutjeharms, J.R.E., Colin de Verdiere, A., Johnson, A., Shillington, F., Freon, P., Brundrit, G., 2001. A regional hydrodynamic model of the Southern Benguela. *S. Afr. J. Sci.* 97, 472–476.
- Pullen, J., Doyle, J.D., May, P., Chavanne, C., Flament, P., Arnone, R.A., 2008. Monsoon surges trigger oceanic eddy formation and propagation in the lee of the Philippine Oslands. *Geophys. Res. Lett.* 35, L07604, doi:10.1029/2007GL033109.
- Qu, T., Mitsudera, H., Yamagata, T., 2000. Intrusion of the North Pacific waters into the South China Sea. *J. Geophys. Res.* 105, 6415–6424.
- Qu, T., Kim, Y.Y., Yaremchuk, M., Tozuka, T., Ishida, A., Yamagata, T., 2004. Can Luzon Strait transport play a role in conveying the impact of ENSO to the South China Sea? *J. Clim.* 17, 3644–3657.
- Qu, T., Du, Y., Meyers, G., Ishida, A., Wang, D., 2005. Connecting the tropical Pacific with Indian Ocean through South China Sea. *Geophys. Res. Lett.* 32, L24609, doi:10.1029/2005GL024698.
- Qu, T., Du, Y., Sasaki, H., 2006. South China Sea throughflow: a heat and freshwater conveyor. *Geophys. Res. Lett.* 32, L23617, doi:10.1029/2006GL028350.
- Quadfasel, D., Kudrass, H., Frische, A., 1990. Deep-water renewal by turbidity currents in the Sulu Sea. *Nature* 348, 320–322.
- Shaw, P.T., 1991. The seasonal variation of the intrusion of the Philippine Sea water into the South China Sea. *J. Geophys. Res.* 96, 821–827.
- Shchepetkin, A.F., McWilliams, J.C., 2005. The regional ocean modeling system (ROMS): a split-explicit, free-surface, topography-following coordinate oceanic model. *Ocean Modelling* 9, 347–404.
- She, J., Klinck, J.M., 2000. Flow near submarine canyons driven by constant winds. *J. Geophys. Res.* 105, 28671–28694.
- Sheremet, V., 2001. Hysteresis of a western boundary current leap across a gap. *J. Phys. Oceanogr.* 31, 1247–1259.
- Stevens, D.P., 1990. On open boundary conditions for three dimensional primitive equation ocean circulation models. *Geophys. Astrophys. Fl. Dyn.* 51, 103–133.



- Sverdrup, H.U., 1947. Wind-driven currents in a baroclinic ocean, with application to the equatorial currents of the eastern Pacific. *Proc. Natl. Acad. Sci. U.S.A.* 33, 318–326.
- Wajsowicz, R.C., 1993. The circulation of the depth-integrated flow around an island with application to the Indonesian Through-flow. *J. Phys. Oceanogr.* 23, 1470–1484.
- Wajsowicz, R.C., 1999. Models of the Southeast Asian Seas. *J. Phys. Oceanogr.* 29, 986–1018.
- Wang, D., Liu, Q., Huang, R., Du, Y., Qu, T., 2006. Interannual variability of the South China Sea throughflow inferred from wind data and an ocean data assimilation product. *Geophys. Res. Lett.* 33, L14605, doi:10.1029/2006GL026316.
- Wang, G., Su, J., Chu, P.C., 2003. Mesoscale eddies in the South China Sea detected from altimeter data. *Geophys. Res. Lett.* 30, 2121, doi:10.1029/2003GL018532.
- Wang, G., Chen, D., Su, J., 2008. Winter eddy genesis in the eastern South China Sea due to Orographic wind jets. *J. Phys. Oceanogr.* 38, 726–732.
- Wang, X., Chao, Y., 2004. Simulated sea surface salinity variability in the tropical Pacific. *Geophys. Res. Lett.* 31, L02302, doi:10.1029/2003GL018146.
- Warner, J.C., Sherwood, C.R., Arango, H.G., Signell, R.P., 2005. Performance of four Turbulence Closure Methods Implemented using a Generic Length Scale Method. *Ocean Modelling* 8, 81–113.
- Wyrtki, K., 1961. *Physical oceanography of the southeast Asian waters*. NAGA Report 2, 195pp., Scripps Inst. of Oceanogr., La Jolla, CA.
- Xue, H., Chai, F., Pettigrew, N., Xu, D., Shi, M., Xu, J., 2004. Kuroshio intrusion and the circulation in the South China Sea. *J. Geophys. Res.* 109, C02017, doi:10.1029/2002JC001724.
- Yuan, D., Han, W., Hu, D., 2006. Surface Kuroshio path in the Luzon Strait area derived from satellite remote sensing data. *J. Geophys. Res.* 111, C11007, doi:10.1029/2005JC003412.
- Yuan, D., Han, W., Hu, D., 2007. Anti-cyclonic eddies northwest of Luzon in summer-fall observed by satellite altimeters. *Geophys. Res. Lett.* 34, L13610, doi:10.1029/2007GL029401.